REPORT DOCUMENTATION PAGE

AFRL-SR-BL-TR-99-

0038

Public reporting burden for this collection of information is estimated to average 1 hour per response, including the time for reviewing instructions, searching existing data sources, gathering and maintaining the data needed, and completing and reviewing the collection of information. Send comments regarding this burden estimate or any other aspect of this collection of information, including suggestions for reducing this burden, to Washington Headquarters Services, Directorate for information Operations and Reports, 1215 Jefferson Davis Highway, Suite 1204, Arlington, VA 22202-4302, and to the Office of Management and Budget, Paperwork Reduction Project (0704-0188), Washington, DC 20503.

1. AGENCY USE ONLY (Leave blank)	2. REPORT DATE	3. REPORT TYPE AND DATES COVERED
		FINAL

4. TITLE AND SUBTITLE
Resonance Enhanced Multiphoton Ionization Spectra of Molecules and Molecular Fragments/Femtosecond Energy- and Angle-resolved Pump-Probe Photoelectron Spectroscopy

5. FUNDING NUMBERS
F49620-95-1-0012
2303/FS
61102F

6. AUTHOR(S)
Vincent McKoy

7. PERFORMING ORGANIZATION NAME(S) AND ADDRESS(ES)
Noyes Laboratory of Chemical Physics
California Institute of Technology
Pasadena CA 91125

8. PERFORMING ORGANIZATION REPORT NUMBER

9. SPONSORING/MONITORING AGENCY NAME(S) AND ADDRESS(ES)
AFOSR/NL
801 N Randolph Street Room 732
Arlington VA 22203-1977

Dr Michael R. Berman

10. SPONSORING/MONITORING AGENCY REPORT NUMBER

11. SUPPLEMENTARY NOTES

12a. DISTRIBUTION/AVAILABILITY STATEMENT

Approved for public release;
distribution unlimited.

12b. DISTRIBUTION CODE

DTIC QUALITY INSPECTED 4

13. ABSTRACT *(Maximum 200 words)*

We have completed studies of ion rotational distributions produced by resonance multiphoton ionization of molecules, molecular fragments and small clusters such as NaH_2O and $NaNH_3$. Our key objective was to provide a robust analysis and prediction of spectral features of interest in related experimental studies and technological applications of laser-driven ionization.

We have also extended our studies of photoelectron spectroscopy from the energy domain to the ultrafast time domain with an emphasis on exploiting femtosecond energy- and angle-resolved photoelectron spectra for real-time mapping of wavepacket motion in molecular systems. We have developed a formulation of time-resolved photoelectron spectroscopy that is well suited for such applications. Results of applications provide compelling evidence of the unprecedented insight that such spectra can provide into both *wavepacket motion* and the evolution of the associated electronic structure. This capability shows significant promise as a probe of wavepacket motion in regions of avoided crossings (nonadiabatic behavior).

14. SUBJECT TERMS	15. NUMBER OF PAGES
Multiphoton ionization of molecules; ultrasensitive detection of trace species; femtosecond pump-probe photoelectron spectroscopy of wavepackets.	16. PRICE CODE

17. SECURITY CLASSIFICATION OF REPORT	18. SECURITY CLASSIFICATION OF THIS PAGE	19. SECURITY CLASSIFICATION OF ABSTRACT	20. LIMITATION OF ABSTRACT
Unclassified	Unclassified	Unclassified	UL (unlimited) SAR (same as report)

Annual Progress Report
(November 1, 1997 – October 31, 1998)

and

Final Technical Report
(November 1, 1994 – October 31, 1998)

AFOSR Grant No. F49620-95-0012

Resonance Enhanced Multiphoton Ionization Spectra of Molecules and Molecular Fragments

and

Femtosecond Energy- and Angle-Resolved Pump-Probe Photoelectron Spectra

Principal Investigator: *Vincent McKoy*
Noyes Laboratory of Chemical Physics
California Institute of Technology
Pasadena, California 91125
Phone: 626-395-6545
Fax: 626-568-8824
E-mail: mckoy@its.caltech.edu

Program Manager: Dr. Michael Berman

19990218024

I. *Introduction*

This report summarizes the progress of our studies of resonance enhanced multiphoton ionization (REMPI) of molecules and molecular fragments and of single-photon ionization of these species by coherent VUV radiation. The focus of these studies has been to provide both a robust description of significant spectral features of interest to applications of this technique such as ultrasensitive detection of trace and transient species and needed insight into the underlying dynamics of these spectra. A summary of our progress in this area is given in the section below.

In the second part of this report we review the progress of our effort to extend our studies of photoelectron spectra from the energy domain, where the premium is on highly resolved molecular ion spectra, to the ultrafast time domain where the emphasis is on exploiting femtosecond energy-and angle-resolved photoelectron spectra for real-time mapping of wavepacket dynamics in small molecular systems. Such time-resolved photoelectron spectra can also provide unprecedented insight into the evolution of the associated electronic structure. The results reported here, in fact, represent a significant advance towards exploiting the full potential of femtosecond energy- and angle-resolved photoelectron spectroscopy as a probe of wavepackets. Such time-, energy-, and angle-resolved photoelectron spectra should be particularly useful for studies of wavepackets in the important cases of avoided crossings (nonadiabatic transitions) and large-amplitude motion. The key to these applications is a robust description of the underlying photoionization amplitudes.

II. *Resonance Enhanced multiphoton Ionization Spectra of Molecules and Molecular Fragments*

1. *Background and Objectives*

Resonance enhanced multiphoton ionization (REMPI) utilizes laser radiation to prepare a molecule in an excited state via absorption of one or more photons and to subsequently ionize that level before it decays. A remarkable feature of REMPI is that the very narrow bandwidth of laser radiation makes it possible to select a specific rotational level in the initial (ground) state and to prepare the excited state of a species of interest in a single rotational level. Thus, by suitable choice of the excitation step, it is possible to selectively ionize a species of interest which occurs in very minor concentrations, without ionizing any other species that may be present. *This conversion of optical selectivity into chemical selectivity makes REMPI one of the most powerful tools for ultrasensitive detection of trace and transient species.* On the more fundamental side, coupled with high-resolution photoelectron detection, REMPI provides ion rotational distributions for ionization of single rotational levels of excited electronic states. Such state-resolved spectra can clearly provide significant insight into the underlying dynamics of molecular photoionization. Other applications of REMPI include its use for studies of state-selective chemistry and for exploring excited-state chemistry at a quantum-state-specific level. Finally, although REMPI has the distinct advantage that a single rotational of an excited electronic state is ionized and that it can be achieved with photon energies less than the ionization potential, studies of photoionization of jet-cooled molecules in their ground electronic states by a single photon of coherent vacuum ultraviolet (VUV) radiation are significant in their own right and highly complementary to those of REMPI.

The key objective of our effort has been to carry out quantitative studies of REMPI of molecules and molecular fragments, as well as of single-photon ionization of these species by coherent VUV radiation, in order to provide a robust description of significant spectral features of interest in related experiments and needed insight into the underlying dynamics of these spectra. Joint theoretical and experimental studies of these ion rotational distributions which are being widely studied by the zero-kinetic-energy (ZEKE)

technique have been a principal focus of our effort.[1] This technique, which is based on the detection of photoelectrons resulting from pulsed-field ionization of very high Rydberg states lying just below an ion threshold, makes it possible to obtain cation distributions with sub-wavenumber resolution. The unprecedented resolution of this ZEKE technique has opened up entirely new vistas in studies of photoionization dynamics, ion spectroscopy, and state-selected ion-molecule reactions. Emerging applications built on the ultra-high resolution of this technique include its use for accurate determination of thermochemically important ionization energies, for characterization of ion rovibrational level structure of large organic molecules, of elemental clusters, and of weakly bound molecular complexes, for probing reactive fragments, and for pump-probe photoelectron studies of wavepacket dynamics. This surge of experimental activity in ultra-high resolution studies of molecular photoelectron spectra continues to raise new theoretical challenges and has provided the stimulus for several of our collaborations with experimental groups in North America and Europe.

2. *Highlights of Accomplishments*

We will now use a few examples to highlight the progress of our studies of ion rotational distributions from REMPI of excited electronic states of molecules and from single-photon ionization of ground state jet-cooled molecules by coherent VUV and extreme ultraviolet (EUV) radiation. Although we will not discuss the numerical and computational details of the procedures used to obtain the molecular photoelectron orbitals needed in these studies, it is essential to recognize that the quantitative determination of the ion rotational distributions of interest here requires the use of molecular photoelectron orbitals which correctly incorporate the angular momentum coupling present in these wave functions. In contrast to atomic photoelectron orbitals, molecular photoelectron orbitals are not angular

momentum eigenfunctions but contain admixtures of angular momenta. This coupling of angular momenta is brought about by the torques associated with the nonspherical potentials of the molecular ions in which the photoelectron moves. This simply reflects the fact that as the photoelectron collides with the ion core, its angular momentum, as well as that of the molecular ion, changes. Such angular-momentum changing collisions between the photoelectron and the ion clearly play a crucial role in determining ion rotational distributions.

In our studies we take the photoelectron orbitals to be solutions of a one-electron Schrödinger equation containing the Hartree-Fock potential of the molecular ion, $V_{ion}(r, R)$,

$$(-\frac{1}{2}\bigtriangledown^2 + V_{ion}(\mathbf{r}, R) - \frac{k^2}{2})\psi_k(\mathbf{r}) = 0, \tag{1}$$

where $k^2/2$ is the photoelectron kinetic energy. We obtain these orbitals numerically using an iterative procedure, based on the Schwinger variational principle, to solve the integral (Lippmann-Schwinger) equation associated with eq. (1). A significant feature of this procedure is that it avoids the integration of the coupled integro-differential equations which normally arise in the numerical solution of Schrödinger equations with nonspherical potentials, V(r, θ, ϕ). The computationally intensive steps of this procedure, which is numerically very stable even at the low photoelectron energies (≈ 0.05 eV) often of interest, are single-center expansions of a large number of multicenter basis functions and operators and subsequent use of these expansions in numerical quadratures of radial integrals.[2]

(a) *Rotationally Resolved REMPI Photoelectron Spectra for H_2O*

We have completed combined theoretical and experimental studies of rotationally resolved, REMPI photoelectron spectra for *low rotational levels* of H_2O at photelectron

energies from about 1 eV to 2.5 eV above threshold. These were the first non-ZEKE rotationally resolved photoelectron spectra for single rotational levels of a polyatomic molecule. While ZEKE photoelectron spectroscopy provides sub-wavenumber resolution in ion rotational distributions, the technique is restricted to the threshold region and does not permit studies at photoelectron energies away from threshold. Studies at higher photoelectron energies can display dynamical behavior which may not be apparent from near-threshold studies. This is particularly true of features that may arise from Cooper minima.

Spectra were measured for $(2 + 1')$ REMPI of specific rotational levels of the $\tilde{C}\ ^1B_1$ (0, 0, 0) state of H_2O using a magnetic bottle photoelectron spectrometer.[3] This spectrometer provided a kinetic energy resolution better than 4 meV. Comparison of the measured and calculated ion distributions is very encouraging and reveals extremely nonatomiclike photoionization dynamics and the influence of Cooper minima in the photoelectron channels. We illustrate these results with spectra for the 4_{13} rotational level of the $\tilde{C}\ ^1B_1$ $(3pa_1)$ state. Fig. 1 shows our calculated rotationally resolved photoelectron spectra along with the measured $(2 + 1')$ REMPI spectra for photoionization of this level. The calculated spectrum is convoluted with a Gaussian detection function with a FWHM of 42 cm^{-1}. These spectra show only type b transitions [ΔK_a = even (odd), ΔK_c = even (odd)], with the most intense transition being $4_{13} \leftarrow 4_{13}$. On the basis of the selection rules governing this transition,[3] i.e., $\Delta K_a + \ell = odd$ and $\Delta K_a + \Delta K_c = even$, this transition must arise from odd partial waves of the photoelectron matrix element. A single-center expansion of the $3pa_1$ orbital shows that it has 14.5 % s, 83.6 % p, and 1.9 % d character. In view of the 84 % p ($\ell = 1$) character of the $3pa_1$ orbital, this intense $4_{13} \leftarrow 4_{13}$ peak in the photoelectron spectra is highly molecular in origin and arises from strong ℓ-mixing in the molecular electronic continuum. Similar behavior is also clearly seen in the mixed peak for the 5_{33} and 6_{15} ionic levels. While the other $\Delta K_a = even$ and $\Delta K_c = even$ ($\ell = odd$)

transitions such as the 3_{31}, 5_{15}, and 4_{31} levels are also dominant, they are mixed with other rotational peaks arising from even ℓ components of the photoelectron matrix element.

To provide some insight into the dynamical aspects of the angular momentum transfer of the photoelectron upon ionization in this system, we show the photoelectron matrix elements for kinetic energies up to 10 eV in Fig. 2. The behavior of these photoionization matrix elements is very nonatomiclike. Surprisingly, multiple Cooper minima are also seen in every continuum channel around 2 eV. These minima are present in the d and f waves of the ka_1 channel, in the p, d, f, and g waves of the kb_1 channel, and in the f and g waves of the kb_2 channel. These Cooper minima strongly deplete the contributions of the even and odd waves over the photoelectron energy range of interest. In the spectra of Fig. 1, the contributions of the odd (especially p and f) waves are much stronger than those of the even waves. The partial wave mixing near threshold is particularly strong.

(b) *REMPI Photoelectron Spectroscopy of Vanadium Dimer*

The elucidation of the electronic and geometric structure of transition metal clusters remains a challenging problem. Although a wealth of spectroscopic information has been obtained on neutral transition metal dimers,[4] very little is known about trimeric and higher clusters. Moreover, with regard to transition metal cluster cations, there is a severe lack of gas-phase spectroscopic data, even for diatomics.

ZEKE photoelectron spectroscopy is a powerful technique for addressing these problems. Recently Yang et al.[5] exploited this technique to study the electronic structure of the vanadium dimer cation. Rotationally resolved ZEKE spectra were obtained by (1 + 1′) REMPI of the A $^3\Pi_u$ excited state of V_2. Striking differences were observed in the ion rotational spectra recorded through the $^3\Pi_{1u}$ spin-orbit component and those recorded

through the $^3\Pi_{2u}$ component, where a wide range of J^+ values are accessed, as opposed to only two in the case of the $^3\Pi_{1u}$ component.

To provide a quantitative description of the underlying dynamics of these features, we have calculated the ZEKE photoelectron spectra of the $X\ ^4\Sigma_g^-$ ground state of V_2^+ for $(1+1')$ REMPI of the $A\ ^3\Pi_u$ state.[6] Fig. 3 shows calculated and measured ZEKE photoelectron spectra for the $A\ ^3\Pi_{1u}$ state of V_2 with the excitation laser tuned to the R(7) line in the $A\ ^3\Pi_{1u} \leftarrow X\ ^3\Sigma_{0g}$ band. Agreement between these measured and calculated spectra is quite encouraging. Due to selection rules, the photoelectron spectra of Fig. 3 for the $A\ ^3\Pi_{1u}$ state show transitions only to the $^4\Sigma_{\frac{1}{2}g}$ spin-orbit component of the ion. Furthermore, since on the basis of parity selection rules,[6] only the e parity component of the $J' = 8$ rotational level is accessed in this R(7) excitation, the number of J^+ rotational levels for the $X\ ^4\Sigma_g^-$ state of V_2^+ is significantly reduced. The agreement between the measured and calculated spectra is reasonable except for the 6.5(f) and 9.5(e) peaks, where our calculated intensities are somewhat stronger than the measured values.

Fig. 4 shows the calculated and measured ZEKE photoelectron spectra for $(1+1')$ REMPI of the $A\ ^3\Pi_{2u}$ state of V_2 with the excitation laser tuned to the R(6) line in the $A\ ^3\Pi_{2u} \leftarrow X\ ^3\Sigma_{1g}^-$ band. For this $A\ ^3\Pi_{2u}$ spin-orbit component, both the $X\ ^4\Sigma_{\frac{1}{2}g}^-$ and $X\ ^4\Sigma_{\frac{3}{2}g}^-$ components of the cation are accessible. Agreement with the measured and calculated spectra is encouraging except for the peak for the $J^+ = 8.5$(e) and 6.5(f) levels which shows a weaker intensity in the calculated spectra. Since the $X\ ^3\Sigma_{1g}^-$ spin-orbit component of the ground state contains both e and f parities for each rotational level, which are assumed to have equal populations, both the e and f parities of the $J' = 7$ rotational level of the $A\ ^3\Pi_{2u}$ component are excited. A wider range of J^+ rotational levels would hence be expected to arise here than for excitation via the $A\ ^3\Pi_{1u}$ component.

(c) *ZEKE Photoelectron Spectra of Sodium-Water and Sodium-Ammonia Clusters*

The energetics, structure, dynamics, and spectroscopy of clusters consisting of neutral or ionic metal atoms and polar solvent molecules are of significant interest in studies of chemical reactions, electron solvation, corrosion, and a wide range of chemical and biological processes. Such clusters, composed of a metal complexed with a variety of solvents, particularly those containing alkali metals, are interesting targets of study with ZEKE-PFI techniques. ZEKE-PFI spectra can be very useful in elucidating the molecular structure and intermolecular force fields of these small clusters. A combination of experimental studies and ab initio calculations can be very effective in unraveling these ZEKE spectra and, hence, in obtaining structural data from these spectra.

We have carried out such a joint study of the ZEKE photoelectron spectra of small $Na(H_2O)_n$ and $Na(NH_3)_n$ clusters with Geoffrey Blake of our Department. Experimentally, it is straightforward to produce these clusters in sufficient quantities to detect with ZEKE-PFI, and the wavelengths required for their spectroscopic investigation are easily generated with dye lasers. We have concentrated on measurements of the ZEKE rotational band contours in the sodium-water and sodium-ammonia complexes and on calculations of these rotational spectra. While agreement between the measured and calculated spectra is quite encouraging, the more significant implication of these results is that they demonstrate how essential calculated spectra are in accounting for the main features of the spectra and their potential for elucidating the molecular structure of the neutral and ionic clusters.[7]

Fig. 5 shows our measured and calculated ZEKE photoelectron spectra for ionization of the $3sa_1$ orbital of the $\tilde{X}\ ^2A_1$ state of NaH_2O by single-photon coherent UV radiation.[7] The calculated spectra were obtained for a photoelectron energy of 50 meV and were convoluted with a Gaussian detector function with a full-width at half-maximum (FWHM)

of 2.2 cm^{-1}. The rotational constants used were derived from the calculated geometry. These are A = 14.157, B = 0.280, and C = 0.275 cm^{-1} for NaH_2O and A^+ = 14.157, B^+ = 0.309, and C^+ = 0.296 cm^{-1} for NaH_2O^+. Comparison of the measured ZEKE spectra with spectra calculated over a wide temperature range suggests a rotational temperature of about 100 K in these experiments. The spectra in Fig. 5 were calculated at this temperature.

Agreement between the measured and calculated spectra is encouraging. The dominant peak in these spectra belongs to P branch transitions ($\Delta N = -1$). The intensity of this peak is due to a band head. Analysis of the calculated spectra shows that $|\Delta N| = 0-4$ transitions contribute 13%, 62%, 15%, 7%, and 3% of the total cross section, respectively. The dominance of $|\Delta N| = 1$ transitions in the ZEKE spectra for photoionization of this $3sa_1$ orbital with its 91% s character is surprising and very nonatomiclike since, on the basis of angular momentum considerations, i.e., $|\Delta N| \leq \ell + 1$, the s($\ell = 0$) wave of the photoelectron drives $|\Delta N| = 1$ transitions. This s $\rightarrow$ s behavior is highly unusual for photoionization of an essentially 3s orbital of sodium where atomiclike propensity rules would suggest a strong p-wave photoelectron matrix element. In fact, our calculated photoelectron matrix elements show an unusually strong s-wave component. Even partial wave components of the photoionization matrix element account for about 70% of the total cross section. Our calculated rotationally resolved photoelectron spectra and the underlying dynamical coefficients account quite well for the principal features of these spectra.[7]

To explore the utility of studies of this kind in elucidating the molecular structure of these neutral and charged clusters, it is instructive to see how changes in the geometry influence the contour of the calculated ZEKE spectra. With such small B and C constants (the A constant does not play a role in determining the "end-over-end" rotational spacing), a slight change in B and C can lead to dramatic change in the spectral profile since, at

a temperature of 100 K, more than 300 transitions contribute to the spectrum. The P branch peak intensity and its underlying band head make this an interesting case study. Fig. 6 shows the calculated spectrum for slight changes in the rotational constants to B = 0.295 and C = 0.283 cm^{-1} for NaH_2O and B^+ = 0.298 and C^+ = 0.286 cm^{-1} for NaH_2O^+ but with the previous value for the A and A^+ rotational constants. This change reflects about a 2% decrease in the Na···O bond length from 2.36 to 2.32 Å. These new rotational constants result in a shift of only about 2 cm^{-1} in the location of the peak of the rotational contour. However, the calculated spectrum shows a dramatically different profile. It is now the Q branch ($\Delta N = 0$) which has the highest peak intensity, even though it contributes only 13% of the cross section, since the similarity of the rotational constants in the neutral and ion precludes formation of P or R band heads. The apparent agreement between these calculated and measured spectra is quite good and may even suggest that the actual rotational constants may be close to these modified values. Comparison of experimental and calculated constants for such clusters can have large uncertainties due to excessive vibrational averaging, present in simple fits to spectra, but which would require an accurate knowledge of the global intermolecular potential energy surface to be included in theoretical treatments. In this context, both the intermolecular stretching and out-of-plane bending modes, may contribute to such certainties here in the rotational constants.

Fig. 7 shows measured and calculated ZEKE photoelectron spectra for ionization of the $3sa_1$ orbital of the $\tilde{X}\ ^2A_1$ state of $NaNH_3$. The dominant peak in the measured and calculated spectra again belongs to P branch transitions and is also due to a band head. The calculated spectra also show a higher intensity profile at large photon energies than seen in the measured spectra. Overall agreement between these spectra, however, is quite good.

Comparison of these spectra with those of NaH_2O can reveal differences due to solvation effects. For example, the $3sa_1$ orbital of $NaNH_3$ has 69% s and 24% p character

about the center-of-mass compared to values of 91% s and 7% p in the case of NaH_2O. This increased delocalization in $NaNH_3$ should lead to changes in the photoelectron spectra. Analysis of the calculated spectrum of Fig. 7 shows that $|\Delta N| = 0 - 4$ transitions contribute 14%, 45%, 23%, 10%, and 7% of the total cross section. Again the dominance of the $|\Delta N| = 1$ branches is due to a surprisingly strong and nonatomiclike s-wave component of the photoionization matrix element. Also, the close to 20% contribution from $|\Delta N| = 3$ and 4 transitions arises from f-wave ($\ell = 3$) components of the photoelectron matrix element. These $|\Delta N| \geq 3$ transitions are about twice as large in $NaNH_3$ than in the NaH_2O complex. Furthermore, with their large Na$\cdots$N and Na$\cdots$O bond lengths, one would expect photoionization of these complexes to occur mainly along the a principal axis. This is indeed the case of NaH_2O where 98% of the cross section is associated with transitions possessing no change in angular momentum about K_a, i.e., $\Delta K = 0$. However, with ammonia as a solvent, only about 60% of the cross section is associated with $\Delta K_a = 0$ transitions. Such differences provide useful insight into the structure of these complexes.

Improved resolution in the measured ZEKE-PFI spectra would provide even greater insight into the structure and dynamics of these clusters. Several routes to such spectra are being explored. For example, in contrast to the pick-up source currently used, laser vaporization offers colder rotational temperatures and would dramatically decrease the number of levels contributing to the ZEKE photoelectron signal. Alternatively, multiphoton ZEKE-PFI studies can be performed in which one laser selects an individual eigenstate of the neutral precursor, which is subsequently excited to a high-n Rydberg level and pulse-field ionized. For these clusters, the first step could involve either electronic excitation of the metal itself or vibrational excitation of intermolecular modes within the solvent. Such efforts are currently underway for these $Na(H_2O)$ and $Na(NH_3)$ complexes.

III. *Femtosecond Energy- and Angle-Resolved Pump-Probe Photoelectron Spectra*

1. *Background and Objectives*

With femtosecond (fs) laser techniques it is now possible to observe nuclear dynamics and to chart the path of chemical reactions in real time.[8-10] A key idea of this femtosecond spectroscopy is to use an ultrashort laser pulse, the pump pulse, to prepare a coherent superposition of molecular eigenstates which evolves in accordance with the time scales for the vibrational ($\sim 10^{-13}$ s) and rotational ($\sim 10^{-10}$ s) motions. The evolution of the wavepacket is then probed by a time-delayed, second ultrashort laser pulse via excitation to a final state which serves as a screen for projection of its dynamics. A variety of detection techniques using different types of final states has been used to probe the ultrafast dynamics of these wavepackets.[8,9,11] These include the use of absorption, laser-induced fluorescence (LIF), multiphoton ionization (MPI), photoelectron spectroscopy, nonlinear degenerate four-wave mixing, time-resolved mass spectroscopy, and stimulated emission pumping.

Of these techniques the use of ionization for detection in femtosecond pump-probe experiments offers several advantages. The ground state of an ion is stable and is often the best characterized excited state of a molecule. Furthermore, detection of ions provides mass and kinetic-energy resolution in time-resolved photodissociation experiments.[12] Ionization also provides photoelectrons and measurements of their spectra as a function of delay time between the pump and probe pulses can provide additional and complementary information on the evolution of the wavepacket in real time. Engel and coworkers[13] have illustrated how well suited photoelectron kinetic energy distributions from pump-probe ionization at different delay times are for mapping wavepacket motion in the diatomic systems Na_2 and NaI. The utility of this technique has been demonstrated experimentally on electronically

excited states of sodium dimer.[14] More recently, wavepacket evolution on the A excited state of NaI has been monitored by detecting both photoions and photoelectrons.[15] Charron and Suzor-Weiner have also presented a wavepacket study of the femtosecond dynamics of this system.[16]

While these studies have clearly served to illustrate the utility and promise of photoelectron spectroscopy for real-time mapping of wavepacket dynamics in small molecular systems, they have generally ignored any dependence of the underlying photoionization amplitudes on geometry and energy in their studies of the energy distributions of the photoelectrons and have also not examined the associated angular distributions of these spectra. Neglecting the dependence of the photoionization matrix element on geometry can generally be a poor approximation if the wavepacket moves through a region of an avoided crossing where the electronic character of the wavefunction can change dramatically or samples a large range of internuclear distances. In fact, the double-minimum state of Na_2 studied by Engel and coworkers[13] and the state of NaI studied by Charron and Suzor-Weiner[12] are both formed by an avoided crossing of two diabatic states. Furthermore, photoelectron angular distributions can be expected to convey richer structural and dynamical information than is contained in angle-averaged energy spectra.

The objective of our effort has been to exploit femtosecond energy- and angle-resolved photoelectron spectra as a probe of wavepacket dynamics. We have developed a formulation of time-resolved photoelectron spectroscopy that is well suited for such applications and have used it to study wavepacket motion in the $^1\Sigma_u^+$ double-minimum state of Na_2. In these studies we use geometry- and energy-dependent photoionization amplitudes derived from calculations employing sophisticated descriptions of the wavefunctions for the double-minimum state and for the molecular photoelectrons of the final ionized state. To illustrate the utility of femtosecond photoelectron spectra for probing both molecular vibrations and rotations in real time, we examine spectra for molecules aligned via a linearly polarized

pump pulse and photoionized by a probe pulse polarized either parallel or perpendicular to the pump pulse.

These results illustrate several key points. First, a robust description of the underlying photoionization amplitudes greatly enhances the utility of femtosecond photoelectron spectroscopy as a probe of wavepacket dynamics. In fact, the use of such photoionization amplitudes is essential if the wavepacket moves through an avoided crossing or samples a large region of internuclear distances. Second, the angular distributions of the photoelectrons are insightful fingerprints of vibrational wavepacket dynamics. Furthermore, the strong dependence of these angular distributions on the relative polarizations of the pump and probe pulses can be readily exploited to monitor molecular alignment.

2. *Highlights of Progress*

(a) *Formulation*

Fig. 8 illustrates key features of the scheme used in our studies of energy- and angle-resolved photoelectron spectra for femtosecond ionization of vibrational wavepackets in the $^1\Sigma_u^+$ double-minimum state of aligned Na_2 molecules. A femtosecond polarized laser pulse of frequency ω_1 prepares a wavepacket on the double-minimum $^1\Sigma_u^+$ state which is then ionized by a time-delayed polarized femtosecond laser pulse of frequency ω_2. The polarized pump pulse produces an aligned distribution of Na_2 molecules (θ_R) since only those molecules with their transition moments $\vec{\mu}$ parallel or nearly parallel to the polarization vector of the pump pulse ($\vec{\epsilon}_{pump}$) are excited. The vibrational and rotational motions of this system with their respective time scales of 10^{-13} and 10^{-10} seconds are monitored via the energy and angular (θ_k, ϕ_k) distributions of photoelectrons produced from ionization of the wavepacket by a pulse with a polarization vector $\vec{\epsilon}_{pump}(\theta_P, \phi_P)$. Both $\vec{\epsilon}_{pump}$ and $\vec{\epsilon}_{probe}$ lie in the yz-plane.

The time-dependent wavefunction for this system can be expanded as

$$\Psi\left(\vec{r},\vec{R},t\right) = \chi_0\left(\vec{R},t\right)\Phi_0\left(\vec{r};R\right) + \chi_e\left(\vec{R},t\right)\Phi_e\left(\vec{r};R\right) + \int d\vec{k}\chi_{\vec{k}}\left(\vec{R},t\right)\Phi_{\vec{k}}^{(-)}\left(\vec{r};\vec{R}\right), \quad (2)$$

where Φ_0, Φ_e, and $\Phi_{\vec{k}}^{(-)}$ are the respective eigenfunctions for the ground, excited, and final ionized states, respectively, χ_0, χ_e, and $\chi_{\vec{k}}$ are the nuclear wavepackets on the individual potential energy surfaces, $\vec{r}$ denotes electronic coordinates, and $\vec{R}$ is the internuclear vector. The interaction between the molecule and the laser fields, $V(t)$, is given by (see fig. 8)

$$\begin{aligned} V(t) &= V_1(t;\theta_R,\phi_R,\omega_1) + V_2(t;\theta_R,\phi_R,\theta_P,\omega_2;\Delta T) \\ &= E_1 f_1(t)\sin(\omega_1 t)\vec{\epsilon}_{pump}\cdot\vec{\mu} + 2E_2 f_2(t-\Delta T)\cos(\omega_2 t)\vec{\epsilon}_{probe}\cdot\vec{\mu}, \end{aligned} \quad (3)$$

where E_1 and E_2 are the electric field amplitudes of the pump and probe pulses, $f_1(t)$ and $f_2(t)$ are the envelopes of these pulses, μ is the electric-dipole operator, and ΔT is the time delay between the pump and probe pulses. With $\Psi(t)$ and $V(t)$ of Eqs. (2) and (3), projection of $\langle\Phi_0(\vec{R})|$, $\langle\Phi_e(\vec{R})|$, and $\langle\Phi_{\vec{k}}^{(-)}|$ onto the Schrödinger equation yields equations of motion for the nuclear wavepackets $\chi_0(\vec{R},t)$, $\chi_e(\vec{R},t)$, and $\chi_{\vec{k}}(\vec{R},t)$

$$i\hbar\frac{\partial}{\partial t}\chi_0(\vec{R},t) = [T_N + V_0(R)]\chi_0(\vec{R},t) + \langle\Phi_0(R)|V_1(t;\theta_R,\phi_R,\omega_1)|\Phi_e(R)\rangle\chi_e(\vec{R},t) \quad (4)$$

$$\begin{aligned} i\hbar\frac{\partial}{\partial t}\chi_e(\vec{R},t) &= [T_N + V_e(R)]\chi_e(\vec{R},t) + \langle\Phi_e(R)|V_1(t;\theta_R,\phi_R,\omega_1)|\Phi_0(R)\rangle\chi_0(\vec{R},t) \\ &\quad + \int d\vec{k}\langle\Phi_e(R)|V_2(t;\theta_R,\phi_R,\theta_P,\omega_2;\Delta T)|\Phi_{\vec{k}}^{(-)}(\vec{R})\rangle\chi_{\vec{k}}(\vec{R},t) \end{aligned} \quad (5)$$

and

$$\begin{aligned} i\hbar\frac{\partial}{\partial t}\chi_{\vec{k}}(\vec{R},t) &= [T_N + V_{ion}(R) + \frac{(k\hbar)^2}{2m}]\chi_{\vec{k}}(\vec{R},t) \\ &\quad + \langle\Phi_{\vec{k}}^{(-)}(\vec{R})|V_2(t;\theta_R,\phi_R,\theta_P,\omega_2;\Delta T)|\Phi_e(R)\rangle\chi_e(\vec{R},t), \end{aligned} \quad (6)$$

where $V_0(R)$, $V_e(R)$, and $V_{ion}(R)$ are the potential energy surfaces for the ground, excited, and ionic states, respectively, and m is the mass of the electron.

For a linearly polarized pulse, the interaction matrix element between the ground and excited states is given by

$$\langle \Phi_e | V_1 \left(t; \theta_R, \phi_R, \omega_1\right) | \Phi_0 \rangle = E_1 f_1(t) \sin(\omega_1 t)\ \mu_{e0} \cos(\theta_R) \tag{7}$$

where μ_{e0} is the electric-dipole matrix element between the ground and excited states. To obtain the coupling matrix element between the excited and ionized states, we write $\Phi_{\vec{k}}^{(-)}(\vec{r}, \vec{R})$ as antisymmetrized product of an ion wavefunction (Na_2^+) and a photoelectron orbital $\phi_{\vec{k}}^{(-)}$. With an expansion of $\phi_{\vec{k}}^{(-)}$ in its partial wave components, $\psi_{k\ell m}$, the coupling matrix element between the excited state Φ_e and the final ionized state can be written as

$$\begin{aligned} &\langle \Phi_{\vec{k}}^{(-)}(\vec{R}) | V_2 \left(t; \theta_R, \phi_R, \theta_P, \omega_2; \Delta T\right) | \Phi_e(\vec{R}) \rangle \\ &\qquad = 2E_2 \cdot f_2(t - \Delta T) \cos(\omega_2 t) \sum_{\ell m} C_{\ell m} Y_{\ell m}(\hat{k}) \end{aligned} \tag{8}$$

These $C_{\ell m}$ coefficients, which are obtained using numerical solutions of the partial wave components $\psi_{k\ell m}$ of the photoelectron orbital, provide the underlying dynamical information for photoionization of an oriented Na_2 molecule.

With a similar expansion of the ion nuclear wavepacket $\chi_{\vec{k}}$ in partial waves about $\hat{k}$, the direction of the photoelectron,

$$\chi_{\vec{k}}\left(\vec{R}, t\right) = \sum_{lm} \chi_{klm}\left(\vec{R}, t\right) Y_{lm}\left(\hat{k}\right), \tag{9}$$

Eqs. (5) and (6) can be written as

$$\begin{aligned} i\hbar \frac{\partial}{\partial t} \chi_e(R,t) &= [T_N + V_e] \chi_e(R,t) + V_{e0} \chi_0(R,t) \\ &+ \int dk k^2 \sum_{\ell m} E_2 f_2(t - \Delta T) \exp(i\omega_2 t) C^*_{\ell m}(k, \theta_R, \phi_R, \theta_P) \chi_{k\ell m}(R,t), \end{aligned} \tag{10}$$

and

$$\begin{aligned} i\hbar \frac{\partial}{\partial t} \chi_{k\ell m}(R,t) &= \left[T_N + V_{ion} + \frac{(k\hbar)^2}{2m}\right] \chi_{k\ell m}(R,t) \\ &+ E_2 f_2(t - \Delta T) \exp(-i\omega_2 t) C_{\ell m}(k, \theta_R, \phi_R, \theta_P) \chi_e(R,t). \end{aligned} \tag{11}$$

where in Eq. (10)

$$V_{e0} = V_{0e} = \langle \Phi_e | V_1 \left(t; \theta_R, \phi_R, \omega_1 \right) | \Phi_0 \rangle. \tag{12}$$

Discretization of the continuum integration in Eq. (10) via a Gaussian quadrature of order N_k leads to coupled equations for $\chi_0(R,t)$, $\chi_e(R,t)$, and the set of partial-wave functions $\{\chi_{k_j \ell m}\}$ for each quadrature point k_j. The coupled equations are solved with a split-operator technique. In the present applications use of 14 Gaussian quadrature points provided converged results.

(b) *Potential curves and dipole matrix elements*

The potential energy curves for the ground states of Na_2 ($X\ ^1\Sigma_g^+$) and of Na_2^+ ($X\ ^2\Sigma_g^+$) were obtained at 19 internuclear distances between 2 and 11 Å from extensive CI calculations. Extensive CI wavefunctions were used for the ground and double-minimum states in the calculation of the dipole-matrix elements for excitation of the ground state and for photoionization of the excited state. Such a wavefunction is essential to describe the $^1\Sigma_u^+$ state of Na_2 which results from an avoided crossing of two adiabatic states.[17] The first of these gives rise to the inner well and is a Rydberg state with about 96 % p character. The outer well arises from the second diabatic state which has considerable ionic character at large distance but whose description changes with nuclear separation. This behavior with nuclear separation results in a dipole-excitation amplitude that is very Franck-Condon in the inner well but changes substantially in the outer well. The very molecular nature of this excited state at very large internuclear distances can be seen in the μ_{ge} shown in Fig. 8.

To obtain the photoionization amplitudes we again employed the CI wavefunction for the double-minimum excited state but used a frozen-core Hartree-Fock description of the wavefunction for the ionized state. In this model the wavefunction is an antisymmetrized

product of Hartree-Fock ion orbitals and a photoelectron orbital that is a solution of a one-electron Schrödinger equation containing the Hartree-Fock potential of the Na_2^+ ion. We have previously developed numerical procedures used to obtain the photoelectron orbitals.[2] The Hartree-Fock wavefunction provides a very adequate description of the Na_2^+ system over the complete range of internuclear distances of interest here.

The changing character of the excited state wavefunction with geometry is expected to result in a significant dependence of the photoelectron matrix elements and hence of the dynamical coefficients $C_{\ell m}$ of Eq. (8) on internuclear distance. In fact, this results in an unusual oscillatory behavior of the $C_{\ell m}$ coefficients with geometry around the barrier and across the outer well. The $|C_{\ell m}|^2$ coefficients for a photoelectron energy of 0.5967 eV and for the polarization vectors of the pump and probe pulses parallel to the molecular axis (only $m = 0$ terms allowed) shown in Fig. 8 illustrate this behavior well.

(c) *Non-Franck-Condon behavior and oscillation of ion signal*

A significant objective of this work is to highlight the importance of incorporating realistic and geometry-dependent photoionization amplitudes in calculations of femtosecond photoelectron spectra for wavepacket motion. An excellent illustration of this arises from noting that all $|C_{\ell m}(k_j, R)|^2$ for all relevant (k_j, ℓ, m) essentially vanish in a narrow range to the left of the potential barrier on the excited state (≈ 4 Å). This suggests that ionization of a wavepacket placed in the inner well by the pump laser should result in a very low photoelectron signal whenever the wavepacket hits this "depleted" region and hence in an oscillatory signal as a function of delay time. This behavior would be highly unusual.

To illustrate this feature we select a pump photon energy of 3.62 eV which is 0.06 eV below the top of the barrier. The lowest vibrational level of the ground state is pumped

with a FWHM 120 fs Gaussian pulse centered at $t = 0$, forming a wavepacket around 3.1 Å directly above the initial wavepacket. This wavepacket immediately begins an oscillatory motion with a period of 347 fs, striking the outer turning point around 4.1 Å, where the ion signal should be very weak, at 158 fs. The effect of the pump pulse is negligible after $t = 145$ fs and hence the excited state population is constant beyond this time. This excited state wavepacket is ionized by a laser pulse with a FWHM of 40 fs, a photon energy of 2.28 eV, and polarization parallel to that of the pump pulse. The total ion signal, obtained as an integral over all photoelectron energies and angles, i.e.,

$$P_{ion} = \int d\Omega_k \int dR \, |\chi_{\vec{k}}(R, t_f)|^2 = \int dk \, k^2 \sum_{\ell m} \int dR \, |\chi_{k\ell m}(R, t_f)|^2, \qquad (13)$$

is shown for several delay times between $t = 121$ fs and 1270 fs in Fig. 2(a). t_f in Eq. (13) is taken sufficiently long after the probe pulse interaction is over. The ion signal exhibits an oscillatory behavior with a period determined by the motion of the wavepacket in the inner well.

To provide further insight into these minima in the ion signal, we show the form of the wavepacket at times of 610, 726, and 842 fs. These times are indicated by (I), (II), and (III) in Fig. (9). At 610 fs the wavepacket is delocalized and the ion signal results from ionization over a wide region of this inner well ((I) in Fig. 9). After passing through the intermediate stage at 726 fs (II), there is a significant accumulation of the wavepacket around 4 Å, the righthand turning point, at 842 fs (III). Depletion of the dynamical coefficients $C_{\ell m}$ results in a dramatic decrease in the ion signal for ionization at this time. A robust description of the photoionization dynamics is clearly essential for capturing this behavior.

(d) *Photoelectron energy distributions*

We next look at the photoelectron energy distributions for ionization of a wavepacket that is formed by a pump pulse with an energy almost equal to the top of the potential barrier in the excited state ($\hbar\omega_1 = 3.68$ eV). Fig. 10 shows the behavior of such a wavepacket formed by a pulse with a FWHM of 120 fs and centered at $t = 0$. It takes the wavepacket about 100 fs to reach the barrier at 4.7 Å where it splits into two components, a lower-energy component that is reflected into the inner well and reaches its inner turning point at $t = 400$ fs and 800 fs and a higher-energy component in the outer well that reaches its outer turning point at $t = 600$ fs and rejoins the inner well component at $t = 1000$ fs. This wavepacket is photoionized by a probe pulse with energy $\hbar\omega_2$ of 2.28 eV and a FWHM of 40 fs. The photoelectron signal in an energy interval $d\epsilon_k$ is given by

$$P_{ion}(\epsilon_k)d\epsilon_k = kd\epsilon_k \int d\Omega_k \int dR\ |\chi_{\vec{k}}(R,t_f)|^2 = kd\epsilon_k \sum_{\ell m} \int dR\ |\chi_{k\ell m}(R,t_f)|^2. \qquad (14)$$

Fig. 11 shows the resulting photoelectron energy distributions as a function of delay time ΔT between the pump and probe pulses and with the polarization vectors of the pump and probe parallel. Characterization of the peaks in this spectrum is straightforward. Fig. 11 shows that the wavepacket moves slowly through the barrier region at around $\Delta T = 200$ and 1000 fs. The large values of the dynamical coefficients $C_{\ell m}$'s sandwiching this barrier region between 4 and 5 Å (see Fig. 8) result in strong photoelectron peaks around 0.6 eV for these delay times of 200 and 1000 fs. A strong peak at very low photoelectron energy ($\sim$ 0.0002 eV) is seen around $\Delta T = 600$ fs when the wavepacket hits the outer turning point near $R = 8.5$ Å where only photoelectrons with low kinetic energy can be ejected since almost all the energy goes into potential energy of Na_2^+. While the signal is less intense for ionization of this wavepacket by a probe pulse polarized perpendicular to the pump pulse, the photoelectron spectrum is very similar to that of Fig. 11.

(e) *Photoelectron angular distributions*

Angular distributions are well-known to provide valuable insight into the underlying dynamics of conventional photoelectron spectra. In time-resolved pump-probe photoelectron spectroscopy, these angular distributions can also be expected to be significant dynamical windows on wavepacket behavior and on the evolving electronic structure. We now report the first results of such studies. These time-domain photoelectron angular distributions are given by

$$A(\theta_k, \Delta T, \epsilon_k) d\epsilon_k = \int dR \mid \sum_{\ell m} \chi_{k\ell m}(R, t_f, \Delta T) Y_{\ell m}(\theta_k, \frac{\pi}{2}) \mid^2 k d\epsilon_k, \tag{15}$$

where θ_k is measured relative to the polarization of the probe pulse. Fig. 12 shows these angular distributions for the probe pulse (2.28 eV) polarized parallel and perpendicular to the pump pulse (3.68 eV) and for a photoelectron energy of 0.5967 eV. In contrast to the similarity of the photoelectron energy distributions, the angular distributions are strikingly different for the "parallel" and "perpendicular" cases. For the parallel case the angular distributions are clearly of the d_{z^2} type, as shown in the inset of Fig. 12, while they show d_{yz} behavior for the perpendicular case. This behavior is consistent with symmetry considerations for the dipole interaction. Fig. 10 shows that the weaker photoelectron signal for ionization at 605 fs comes from the inner well region where the photoionization amplitude is low while the stronger signal at ΔT of 968 fs comes from the barrier region as the wavepacket returns from the outer basin. In this barrer region the wavepacket moves slowly and the ionization amplitudes are large. The corresponding partial wave components of the ion wavepacket $\chi_{k_j \ell m}(R, t)$ provide very graphic images of the photoionization dynamics of these wavepackets. Some examples are shown in Fig. 13.

The strong dependence of the photoelectron angular distributions on the angle between the molecular axis and the polarization of the probe pulse makes these distributions a valuable real-time probe of molecular rotation. In the present example, consider a molecule

rotating in the yz-plane and oriented at an angle θ_R relative to the z-axis at a probe time ΔT. For ionization by a probe pulse polarized along the z-axis, the angular distributions in the direction θ_k should behave like

$$A(\theta_k;\theta_R(\Delta T)) = \cos^2\theta_R \times (d_{z^2} - \text{distribution}) + \sin^2\theta_R \times (d_{yz} - \text{distribution}) + \cos\theta_R \sin\theta_R \times (\text{cross term}). \quad (16)$$

The photoelectron signal hence depends strongly on the position of the detector. For example, for the detector along the z-axis, there should be a significant photoelectron signal (due to the d_{z^2} distribution) only for those delay times when the molecules are lined up along the z-axis. Two such peaks should be recorded in a single rotational period. On the other hand, for those delay times when the molecule lies along 45°, a significant signal should be detected due to the d_{yz}-type distributions. Four such large signals should be observed in a single period. With the detector along the y-axis, only the d_{yz}-type distributions would result in a significant photoelectron signal. This peak signal should occur for $\theta_R(\Delta T) \approx 45°$. No significant signal is expected from the d_{z^2}-type distributions. This strong dependence of the photoelectron signal on delay time can be used for real-time mapping of molecular rotation and can be a valuable supplement or alternative to LIF detection.[10]

(f) *Outlook*

This study represents a significant advance towards exploiting the full potential of femtosecond photoelectron spectroscopy as a probe of wavepacket dynamics. The femtosecond energy- and angle-resolved photoelectron spectra of these studies constitute very compelling evidence of the unprecedented insight that such spectra can provide into both wavepacket motion and the evolution of the associated electronic structure. These time-,

energy-, and angle-resolved photoelectron spectra should be particularly useful for studies of wavepackets in the important cases of avoided crossings and large-amplitude motion. Because these studies must rely on a robust description of the underlying photoionization amplitudes, applications to small polyatomic systems should be most rewarding. Such studies of femtosecond energy- and angle-resolved photoelectron spectra in small polyatomic systems are underway.

References

[1] See, for example, K. Müller-Dethlefs, E. R. Grant, K. Wang, V. McKoy, and E. W. Schlag, Adv. Chem. Phys. Vol. XC, pp. 1–104, 1995.

[2] R.R. Lucchese, K. Takatsuka, and V. McKoy, Phys. Rept. **131**, 147 (1986).

[3] W. L. Glab, P. T. Glynn, P. M. Dehmer, J. L. Dehmer, K. Wang, and V. McKoy, J. Chem. Phys. **106**, 5779 (1997).

[4] M. D. Morse, Advances in Metal and Semiconductor Clusters, Vol. I (JAI, Greenwich, 1993).

[5] D. S. Yang, A. M. James, D. M. Rayner, and P. A. Hackett, J. Chem. Phys. **102**, 3129 (1995).

[6] K. Wang and V. McKoy, Chem. Phys. **207**, 309 (1996).

[7] K. Wang, D. A. Rodham, V. McKoy, and G. A. Blake, J. Chem. Phys. **108**, 4817 (1998).

[8] A. H. Zewail, *Femtochemistry: Ultrafast Dynamics of the Chemical Bond*, Vols. 1 and 2 (World Scientific, Singapore, 1994).

[9] *Femtosecond Chemistry*, edited by J. Manz and L. Wöste (VCH, Weinheim, 1995).

[10] M. Dantus, R. M. Bowman, and A. H. Zewail, Nature **343**, 737 (1990).

[11] *Chemical Reactions and Their Control on the Femtosecond Time Scale*, XXth Solvay Conference on Chemistry, edited by P. Gaspard, I. Burghard, I. Prigogine, and S. A. Rice, Advances in Chemical Physics 101 (Wiley, New York, 1997).

[12] D. Zhong and A. H. Zewail, J. Phys. Chem. **102**, 4031 (1998).

[13] See, for example, M. Braun, Ch. Meier, and V. Engel, J. Chem. Phys. **105**, 530 (1996).

[14] A. Assion, M. Geisler, J. Helbing, V. Seyfried, and T. Baumert, Phys. Rev. A **54**, R4605 (1996).

[15] C. Jouvet, S. Martrenchard, D. Solgadi, C. Dedonder-Lardeux, M. Mons, G. Grégoire, I. Dimicoli, F. Piuzzi, J. P. Visticot, J. M. Mestdagh, P. D'Oliveira, P. Meynadier, and M. Perdrix, J. Phys. Chem. **101**, 2555 (1997).

[16] E. Charron and A. Suzor-Weiner, J. Chem. Phys. **108**, 3922 (1998).

[17] D.L. Cooper, R. F. Barrow, J. Verges, C. Effantin, and J. D'Incan, Can. J. Phys. **62**, 1543 (1984).

Captions

Fig. 1 Ion rotational distributions for (2+1′) REMPI of H_2O via the 4_{13} rotational level of the $C\ ^1B_1$ $(3pa_1)$ state. Only type b transitions (δK_a and ΔK_c = odd or ΔK_a and ΔK_c = even) are allowed. The selection rule is $\Delta K_a + \ell$ = odd. The photoelectron energy is about 0.85 eV.

Fig. 2 Partial wave components of the photoionization matrix element for the $3pa_1$ orbital ($\approx$ 14% s, 84 % p) of the $C\ ^1B_1$ state of H_2O.

Fig. 3 The (a) measured and (b) calculated PFI-ZEKE photoelectron spectra for (1+1′) REMPI via the R(7) line of the $A\ ^3\Pi_{1u} \leftarrow X\ ^3\Sigma^-_{0g}$ band. The e/f labels indicate the parity of the ion rotational levels.

Fig. 4 The (a) measured and (b) calculated PFI-ZEKE photoelectron spectra for (1+1′) REMPI via the R(6) line of the $A\ ^3\Pi_{2u} \leftarrow X^3\Sigma^-_{1g}$ band. The e/f labels indicate the parity of the ion rotational levels. The calculated spectrum is convoluted with a Gaussian detection function with an FWHM of 1.75 cm^{-1} and assumes a kinetic energy of 50 meV.

Fig. 5 (a) Computed ZEKE photoelectron spectra for the ground state of $Na(H_2O)$ with calculated molecular geometries ($Na\cdots O$ and $Na^+\cdots O$ bond lengths of 2.355 Å and 2.230 Å, respectively); (b) measured ZEKE spectra of Geoffrey Blake and coworkers.

Fig. 6 (a) Computed ZEKE photoelectron spectra for the ground state of $Na(H_2O)$ with calculated molecular geometries ($Na\cdots O$ and $Na^+\cdots O$ bond lengths of 2.32 Å and 2.270 Å, respectively); (b) measured ZEKE spectra of Geoffrey Blake and coworkers.

Fig. 7 (a) calculated and (b) measured ZEKE-PFI photoelectron spectra for $NaNH_3$ at a rotational temperature of 100 K. The calculated spectrum assumed rotational constants calculated at equilibrium geometry.

Fig. 8 Potential surfaces of Na_2. The transition matrix elements are superposed. The photoionization amplitude shown is defined as $\left|\widetilde{C}_{k_j \ell m}\right|^2 = \left|k_j \sqrt{w_j} C_{\ell m}(k, \theta_R, \phi_R, \theta_P)\right|^2$. w_j is the quadrature weight at k_j. The scales for μ_{ge} and $|\tilde{C}_{\ell m}|^2$ are to the right.

Fig. 9 (a) Oscillatory behavior of the total ion signal from a wavepacket confined in the inner potential basin. (b) The spatial distribution of the wavepackets associated with the total ion signals at the points (I), (II), and (III) marked in (a). The minima of the ion signal are formed by the packet that is localized at the right-hand turning point, where the ionization amplitudes are depleted.

Fig. 10 Spatio-temporal distribution of the wavepacket pumped to the top of the barrier on the excited state. The zone between the two dotted lines indicates the potential barrier region where the dipole-ionization amplitudes are large and the wavepacket moves slowly.

Fig. 11 Photoelectron signal versus kinetic energy and delay-time for a packet with energy almost at the top of the potential barrier and for parallel polarizations of the pump and probe pulses.

Fig. 12 (a) Photoelectron angular distributions as a function of the delay time for parallel polarizations of the pump and probe pulses. The inset shows a polar-coordinate (θ_k) description at delay times of $\Delta T = 605$ and 968 fs. (b) As in (a) but for the probe pulse polarized perpendicular to the pump pulse.

IV. *Publications*

1. Das, R, Wu, C., Mihill, A.G., Poliakoff, E.D., Wang, K., and McKoy, V., *Alignment of Photoions Far From Threshold*, J. Chem. Phys. **101**, 5402 (1994)

2. Choi, H.C., Rao, R.M., Mihill, A.G., Kakar, S., Poliakoff, E.D., Wang, K., and McKoy, V., *Energy Dependence of Photoion Rotational Distributions of N_2 and CO*, Phys. Rev. Lett. **72**, 44 (1994)

3. Milan, J., Buma, M.J., de Lange, C.A., Wang ,K., and McKoy, V., *Rotationally Resolved Photoelectron Spectroscopy of the* $[a\ ^1\Delta]3d\pi^2\Phi$ *Rydberg States of the SH Radical*, J. Chem. Phys. **103**, 3262 (1995)

4. Wang, K., and McKoy, V., *High Resolution Photoelectron Spectroscopy of Molecules*, Annual Rev. of Phys. Chem. **46**, 275 (1995)

5. Wang, K. and McKoy, V., *Threshold Photoelectron Spectroscopy of the* $A\ ^2\Pi$ *State of* CO^+, J. Chem. Phys. 99, 1643(1995)

6. Wang, K., and McKoy, V., *Ion Distributions for Resonance Enhanced Multiphoton Ionization of* $C\ell O$, J. Phys. Chem. **99**, 172 (1995)

7. Wang, K., and McKoy, V., *Rotationally Resolved Photoelectron Spectra at Near-Threshold Kinetic Energies*, High Resolution Laser Photoionization and Photoelectron Studies, pp. 281-329, edited by I. Powis, T. Baer, and C.Y. Ng (Wiley, 1995)

8. Müller-Dethlefs, K., Grant, E.R., Wang, K., McKoy, V., and Schlag, E.W. *ZEKE-Spectroscopy: Very High Resolution Spectroscopy With Photoelectrons*, Advances in Chemical Physics Vol. XC, pp. 1-104, Edited by I. Prigogine and Stuart A. Rice (Wiley, 1995)

9. Das, R., Wu, C., Mihill, A.G., Poliakoff, E.D., Wang, K., and McKoy, V., *Photoion Alignment: Chemical Signatures 200 eV Above Threshold*, J. Phys. Chem. **99**, 1741 (1995)

10. Poliakoff, E.D., Choi, H.C., Rao, R.M., Mihill, A.G., Kakar, S., Wang, K. and McKoy, V., *Photoion Rotational Distributions from Near-Threshold to Deep in the Continuum*, J. Phys. Chem. **103**, 1773 (1995)

11. Wang, K., and McKoy, V., *Threshold (ZEKE) Photoelectron Spectroscopy of the a* $^3\Sigma^+$ *State of* NO^+, J. Chem. Phys. **104**, 3433 (1996)

12. Wales, N.P.L., Buma, W.J., deLange, C.A., Lefebvre-Brion, H., Wang, K., and McKoy, V., *ZEKE-Pulsed Field Ionization and Resonance Enhanced Multiphoton Ionization Photoelectron Spectroscopy: Ionization Dynamics of Rydberg States in HBr*, J. Chem. Phys. **104**, 4911 (1996)

13. Rao, R.M., Poliakoff, E.D., Wang, K., and McKoy, V., *Global Franck-Condon Breakdown Resulting from Cooper Minima*, Phys. Rev. Lett. **76**, 2660 (1996)

14. Rao, R.M., Poliakoff, E.D., Wang, K., and McKoy, V., *Molecular Photoioniation as a Probe of Vibrational-Rotational-Electronic Correlations*, J. Chem. Phys. **104**, 9654 (1996)

15. Glab, W.L., Glynn, P.T., Dehmer, P.M., Dehmer, J.L., Wang, K., and McKoy, V., *Rotationally Resolved Energy-Dispersive Photoelectron Spectroscopy of* H_2O*: Photoionization of the* $\tilde{C}$ *(0, 0, 0) State at 355 nm*, J. Chem. Phys. **106**, 5779 (1997)

16. Milan, J.B., Buma, W.J., de Lange, C.A., Wang, K., and McKoy, V., *Rotationally Resolved Multiphoton Ionization Photoelectron Spectroscopy of the* $[a\ ^1\Delta]3d\pi\ ^2\Phi$ *and* $[a\ ^1\Delta]5p\pi\ ^2\Phi$ *Rydberg State of the SH Radical*, J. Chem. Phys. **107**, 2782 (1997)

17. Wang, K., Rodham, D.A., McKoy, V., and Blake, G.A., *High Resolution ZEKE-PFI Photoelectron Spectra of the Na (H_2O) Complex*, J. Chem. Phys., **108**, 4817 (1998)

18. Arasaki, Y., Takatsuka, K., Wang, K., and McKoy, V., *Femtosecond Energy-and Angle-Resolved Photoelectron Spectra*, Chem. Phys. Lett., in press (1999)

V. *Personnel Supported*

Principal Investigator: Vincent McKoy, Professor of Theoretical Chemistry

Research fellow: Dr. Kwanghsi Wang

Undergraduate: Evan Reed

VI. *Interactions/Transitions*

1. Presentation: *High-Resolution Laser Induced Photoionization in Molecules*, Invited Talk at the International Workshop on Photoionization, San Francisco, October 1994

2. Presentation: *Ion Rotational Distributions at Near Threshold Photoelectron Energies*, Invited Talk at Emory University (Atlanta, GA), March 1995

3. Presentation: *Ion Rotational Distributions at Low and High Photoelectron Energies*, Invited Talk at the International Symposium on Atomic and Molecular Dynamics in Photoionization, Quebec (Canada), July 1995

4. Presentation: *Ion Rotational Distributions at Low Photoelectron Energies*, Invited Talk at the 23rd International Symposium on Free Radicals, Victoria (Canada), August 1995

5. Presentation: *Ion Rotational Distributions at Near-Threshold Photoelectron Energies*, Invited Talk at the Institute for Molecular Science, Okazaki (Japan), December 1995

6. Presentation: *Highly State-Resolved Studies of Molecular Photoelectron Spectra*, Invited Talk at the Department of Chemistry, UCLA, May 1996

7. Presentation: *Ion Rotational Distributions at Near-Threshold Photoelectron Energies*, Invited talk at the University of Amsterdam, The Netherlands, September 1996.

8. Presentation: *State-Resolved Studies of Molecular Photoionization*, Invited talk at the University of Utrecht, Utrecht, The Netherlands, September 1996.

9. Presentation: *Ion Distributions at Low-Photoelectron Energies*, Invited Talk at the International Workshop on Photoionization Dynamics, Rydberg States and Large-Amplitude Motion, York, United Kingdom, November 1996.

10. Presentation: *Ab initio ZEKE Spectra*, Invited Talk at the Ciba Foundation/Royal Society Discussion Meeting on The Future of Rydberg Spectroscopy, London, United Kingdom, November 1998.

11. Presentation: *Studies of Molecular Photoelectron Spectra at Close-to-Threshold Energies*, Invited Talk at the International Workshop on New Theoretical Concepts in ZEKE Spectroscopy, Kreuth, Germany, July 1997.

12. Presentation: *Mapping Wavepacket Dynamics with Femtosecond Pump-Probe Photoelectron Spectroscopy*, Invited Talk at the Gordon Conference on Electron Spectroscopy, New Hampshire, July 1998.

13. Advisory: Member, Wright Laboratory Board of Visitors, Independent Strategic Assessment Group (to Gen. Richard Davis), 1996-1998.

Inventions: None

Honors

B. Vincent McKoy: Fellow, American Physical Society, 1986- ; Speaker, Distinguished Lecture Series, Louisiana State University, Baton Rouge, 1997.

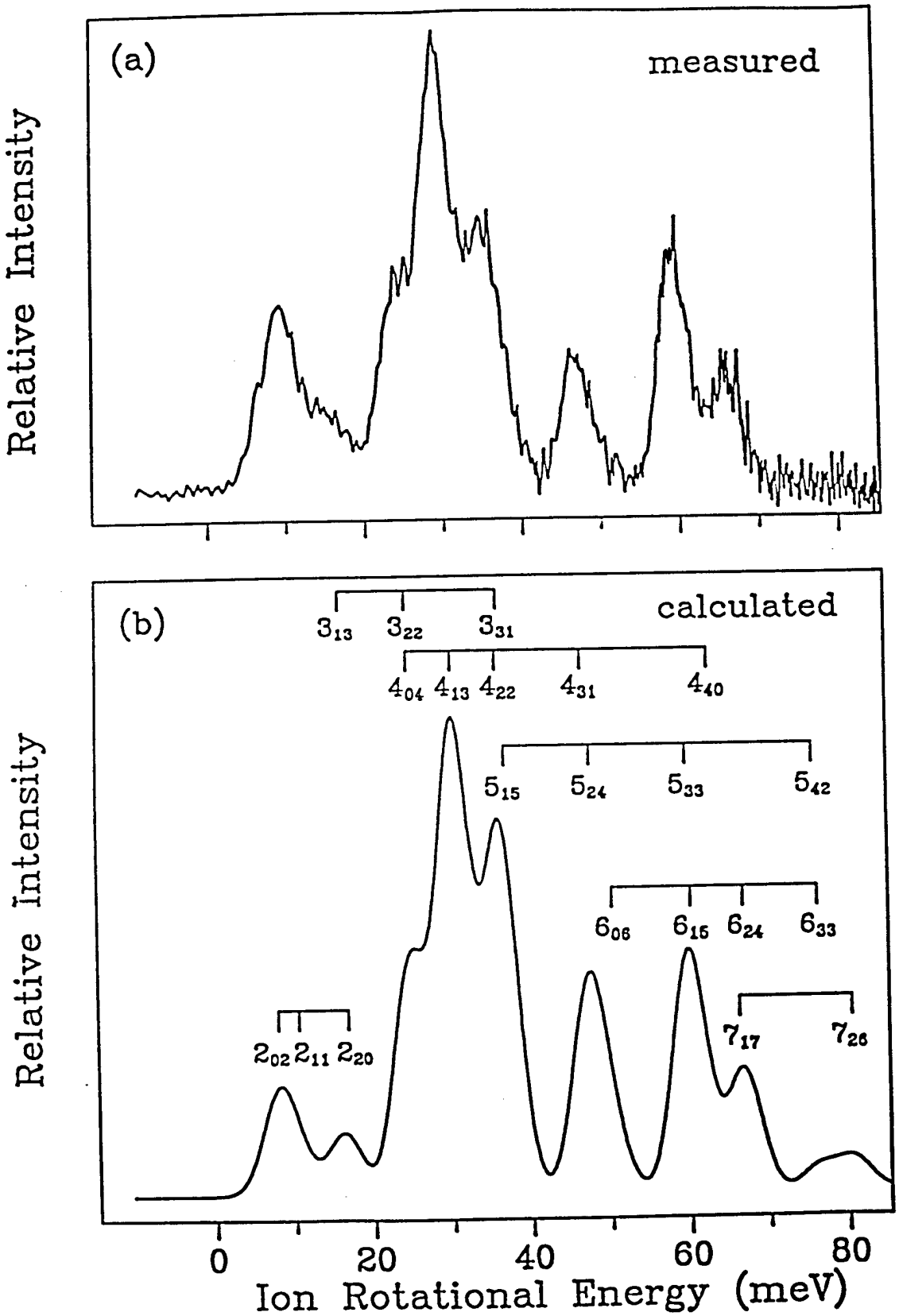
(a)
measured
Relative Intensity
(b)
calculated
3_{13} 3_{22} 3_{31}
4_{04} 4_{13} 4_{22} 4_{31} 4_{40}
5_{15} 5_{24} 5_{33} 5_{42}
6_{06} 6_{15} 6_{24} 6_{33}
7_{17} 7_{26}
2_{02} 2_{11} 2_{20}
Relative Intensity
0
20
40
60
80
Ion Rotational Energy (meV)

Fig. 1

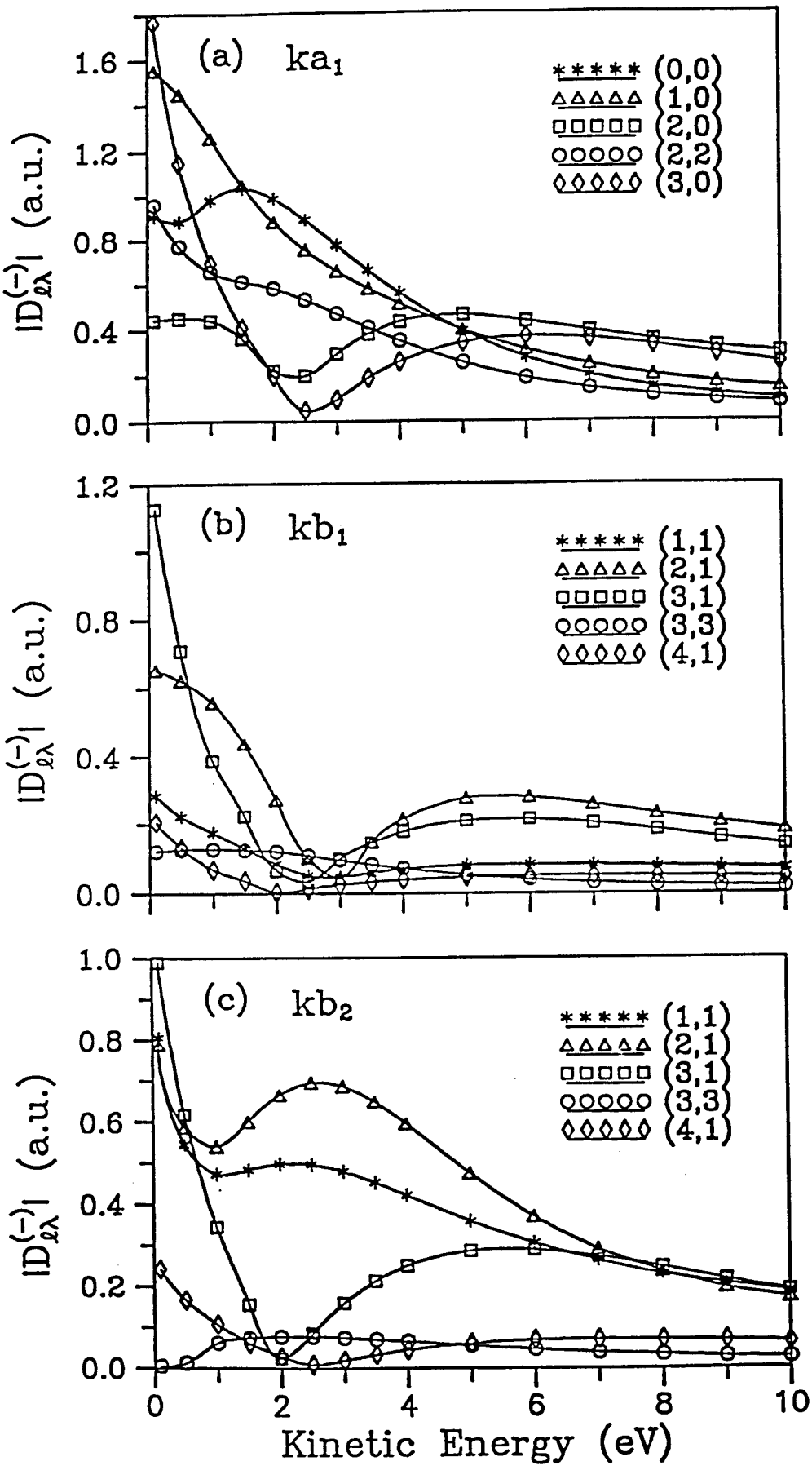
(a) ka_1
(0,0)
(1,0)
(2,0)
(2,2)
(3,0)
(b) kb_1
(1,1)
(2,1)
(3,1)
(3,3)
(4,1)
(c) kb_2
(1,1)
(2,1)
(3,1)
(3,3)
(4,1)
$|D^{(-)}_{\ell\lambda}|$ (a.u.)
Kinetic Energy (eV)

Fig. 2

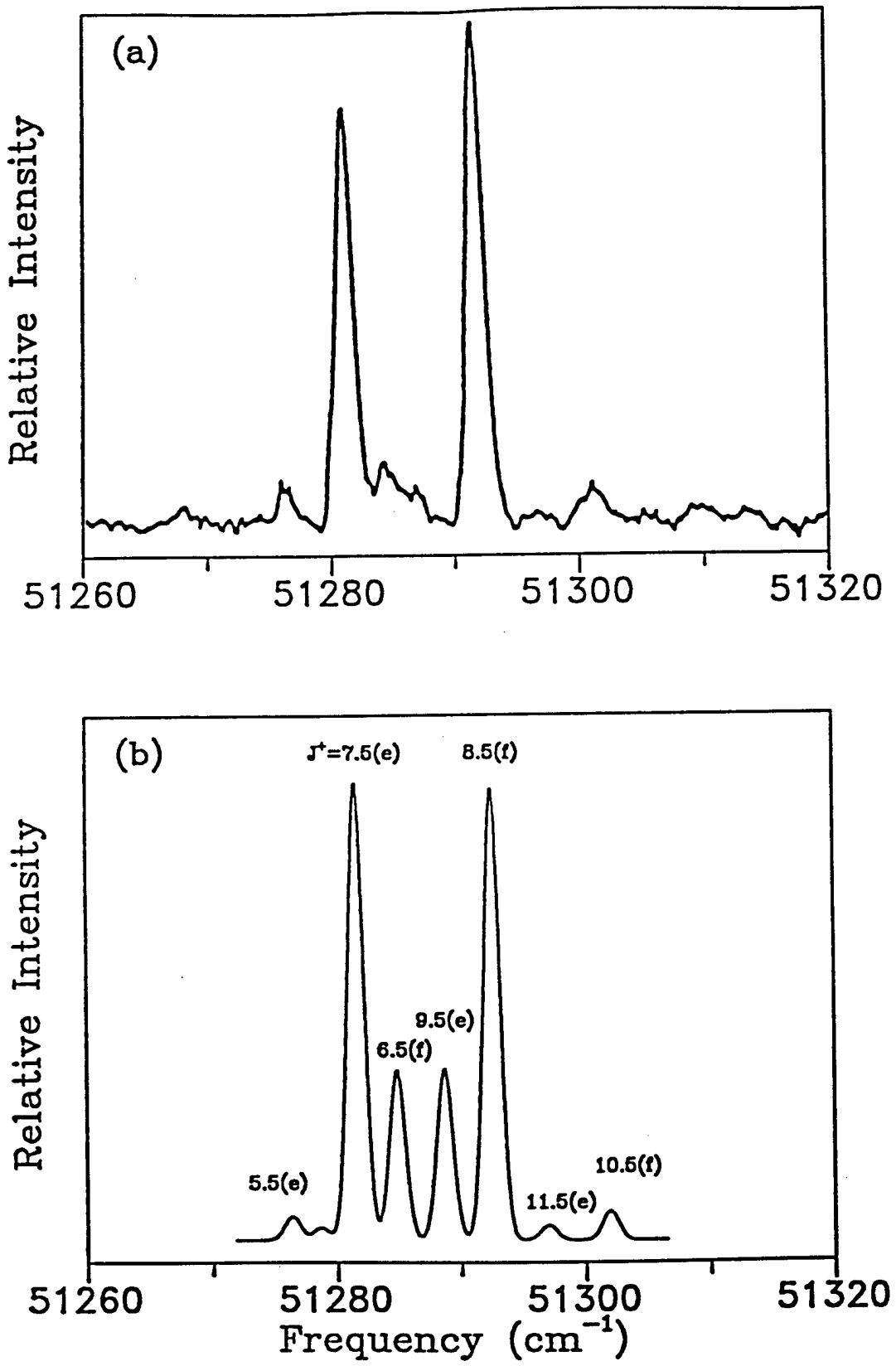
(a)
Relative Intensity
51260
51280
51300
51320
(b)
J'=7.5(e)
8.5(f)
9.5(e)
6.5(f)
5.5(e)
10.5(f)
11.5(e)
Relative Intensity
51260
51280
51300
51320
Frequency (cm^{-1})

Fig. 3

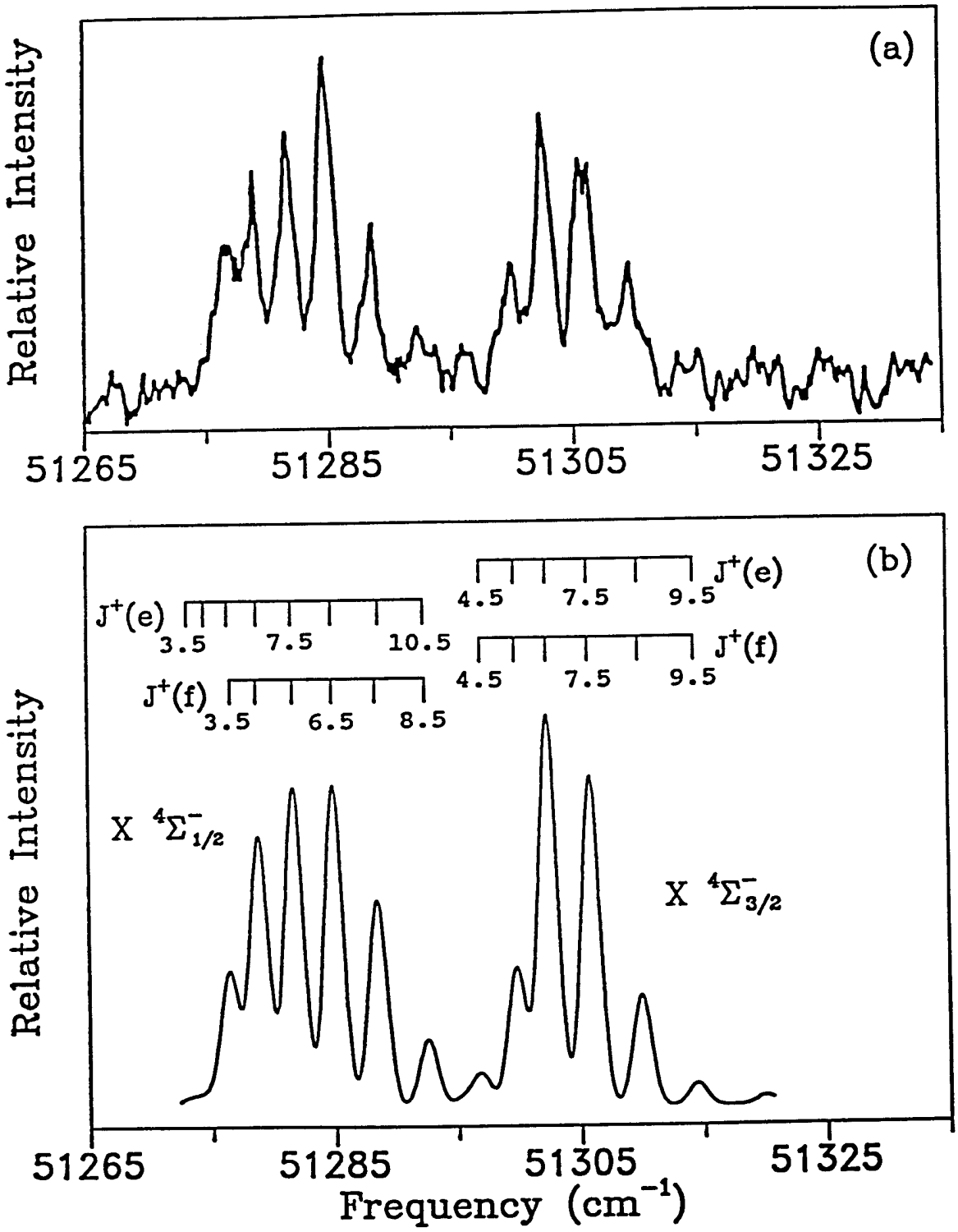
(a)
Relative Intensity
51265
51285
51305
51325
(b)
J+(e)
4.5
7.5
9.5
J+(e)
3.5
7.5
10.5
J+(f)
4.5
7.5
9.5
J+(f)
3.5
6.5
8.5
X 4Σ-1/2
X 4Σ-3/2
Relative Intensity
51265
51285
51305
51325
Frequency (cm-1)

Fig. 4

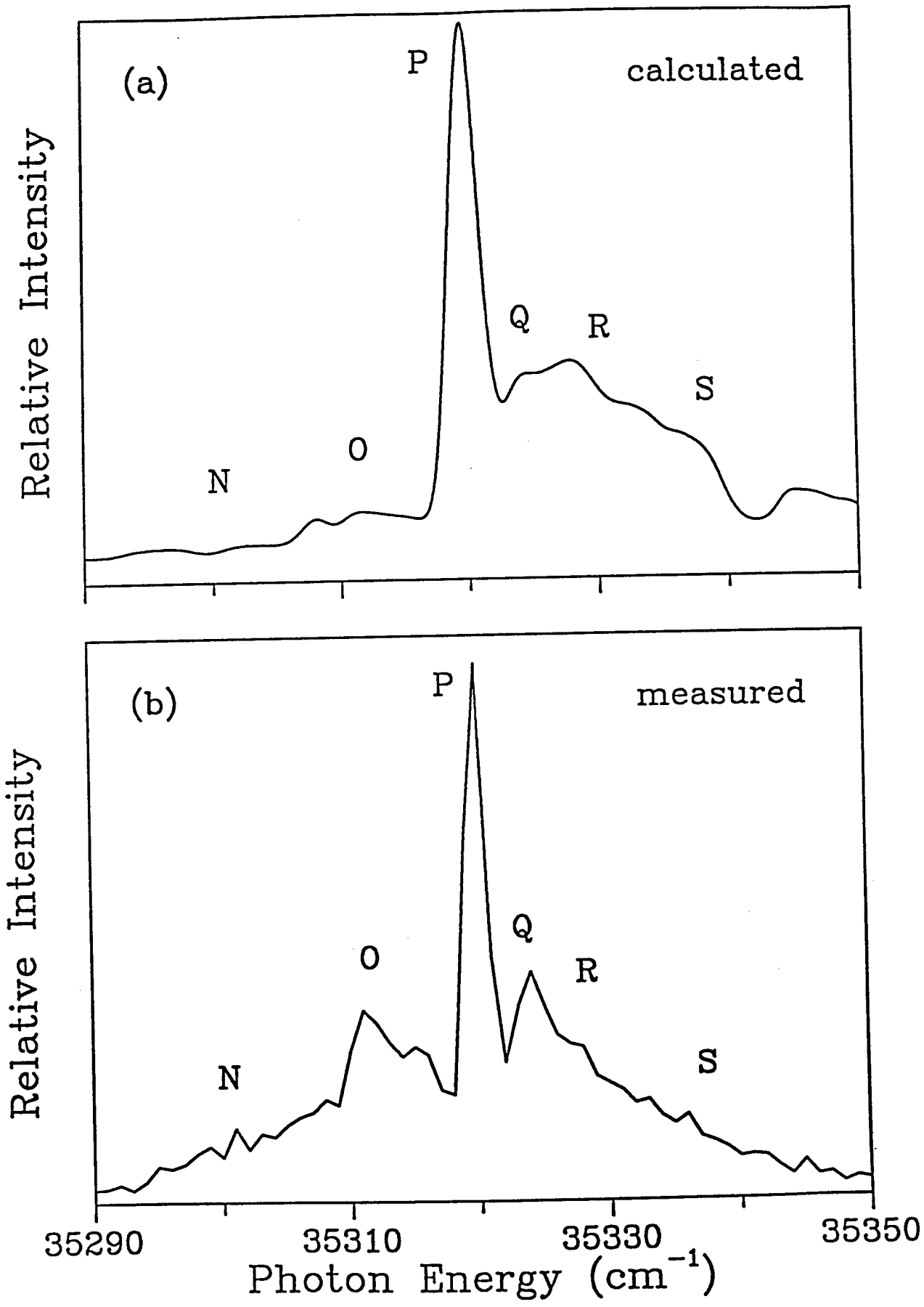
(a)
calculated
P
Q
R
S
O
N
Relative Intensity
(b)
measured
P
Q
R
S
O
N
Relative Intensity
35290
35310
35330
35350
Photon Energy (cm^{-1})

Fig. 5

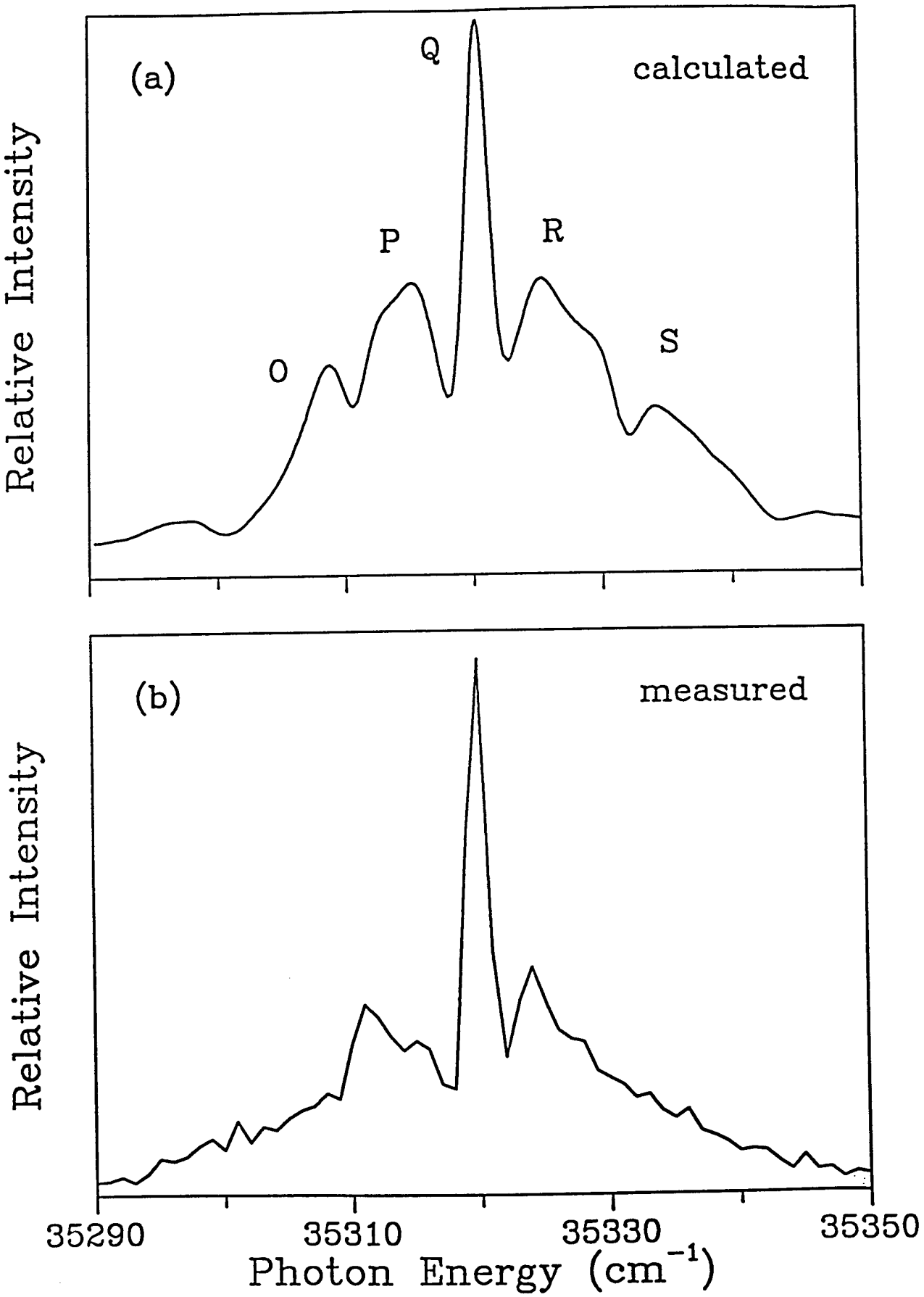
(a)
calculated
Q
P
R
O
S
Relative Intensity
(b)
measured
Relative Intensity
35290
35310
35330
35350
Photon Energy (cm^{-1})

Fig. 6

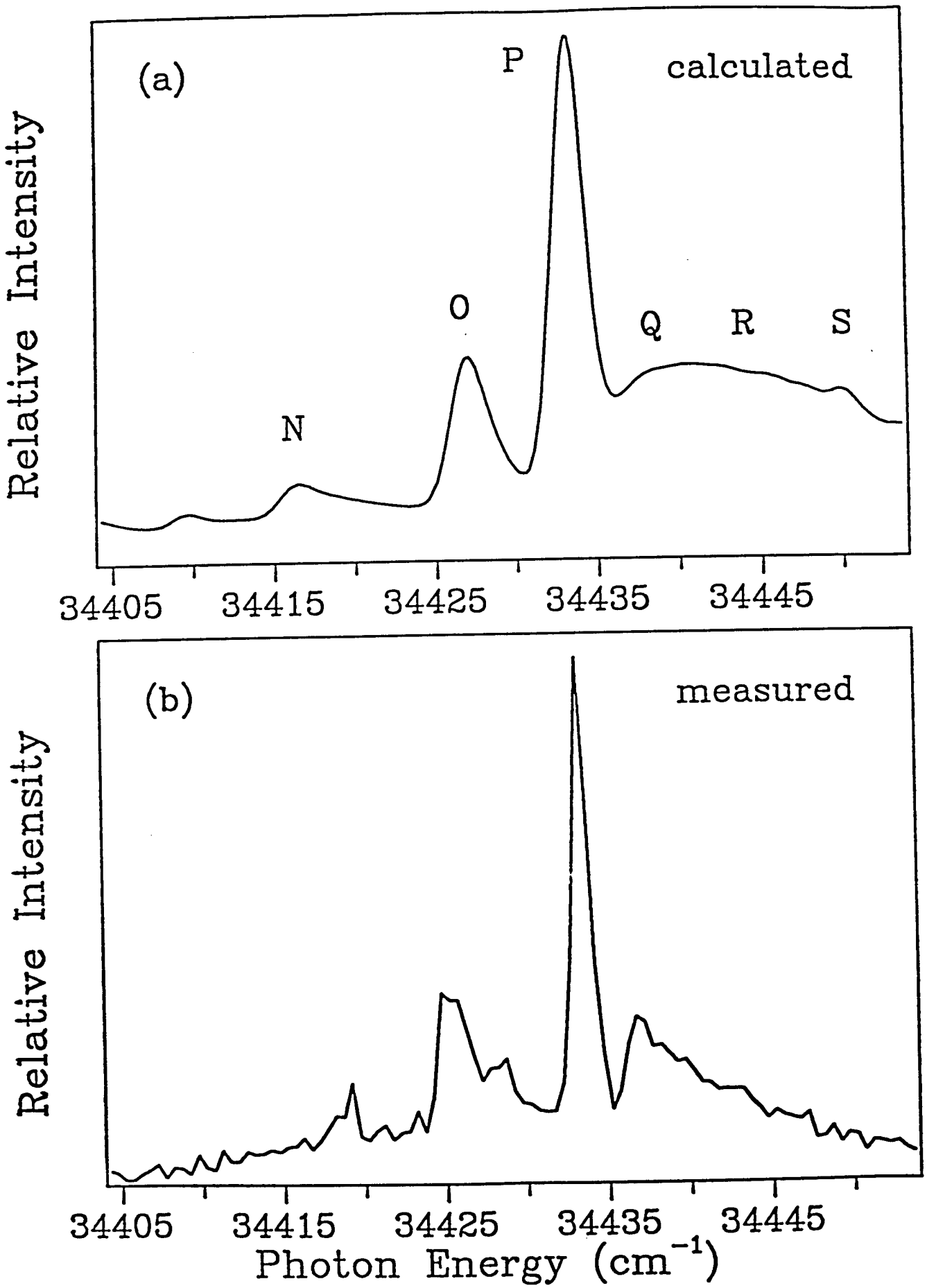
(a)
calculated
P
O
N
Q
R
S
Relative Intensity
34405
34415
34425
34435
34445
(b)
measured
Relative Intensity
34405
34415
34425
34435
34445
Photon Energy (cm^{-1})

Fig. 7

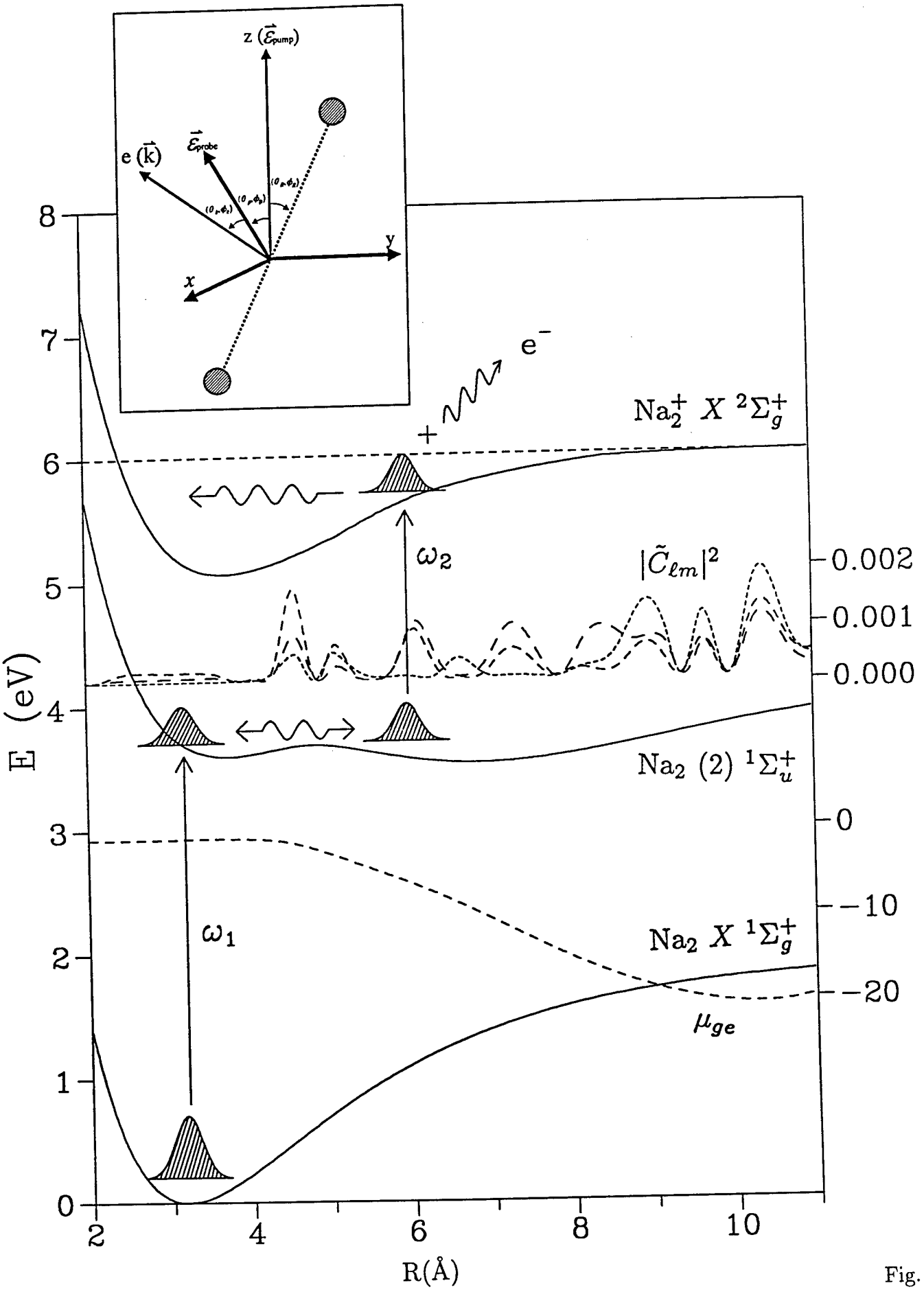
z ($\vec{\mathcal{E}}_{pump}$)
$\vec{\mathcal{E}}_{probe}$
e ($\vec{k}$)
y
x
e$^-$
Na_2^+ $X\ ^2\Sigma_g^+$
ω_2
$|\tilde{C}_{\ell m}|^2$
0.002
0.001
0.000
Na_2 (2) $^1\Sigma_u^+$
ω_1
Na_2 $X\ ^1\Sigma_g^+$
μ_{ge}
0
−10
−20
E (eV)
R(Å)
0
1
2
3
4
5
6
7
8
2
4
6
8
10

Fig. 8

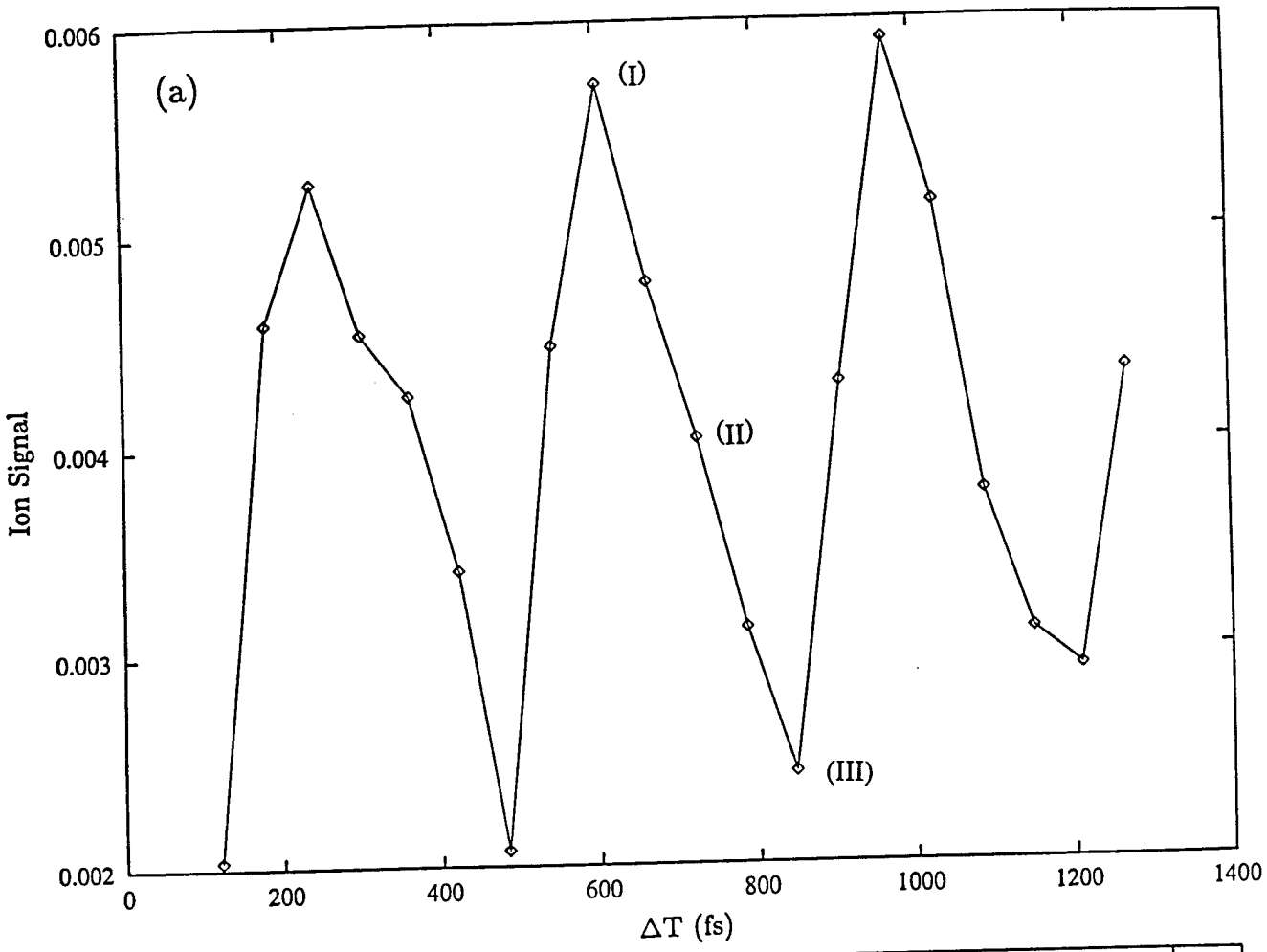
(a)
(I)
(II)
(III)
Ion Signal
0.006
0.005
0.004
0.003
0.002
0
200
400
600
800
1000
1200
1400
ΔT (fs)

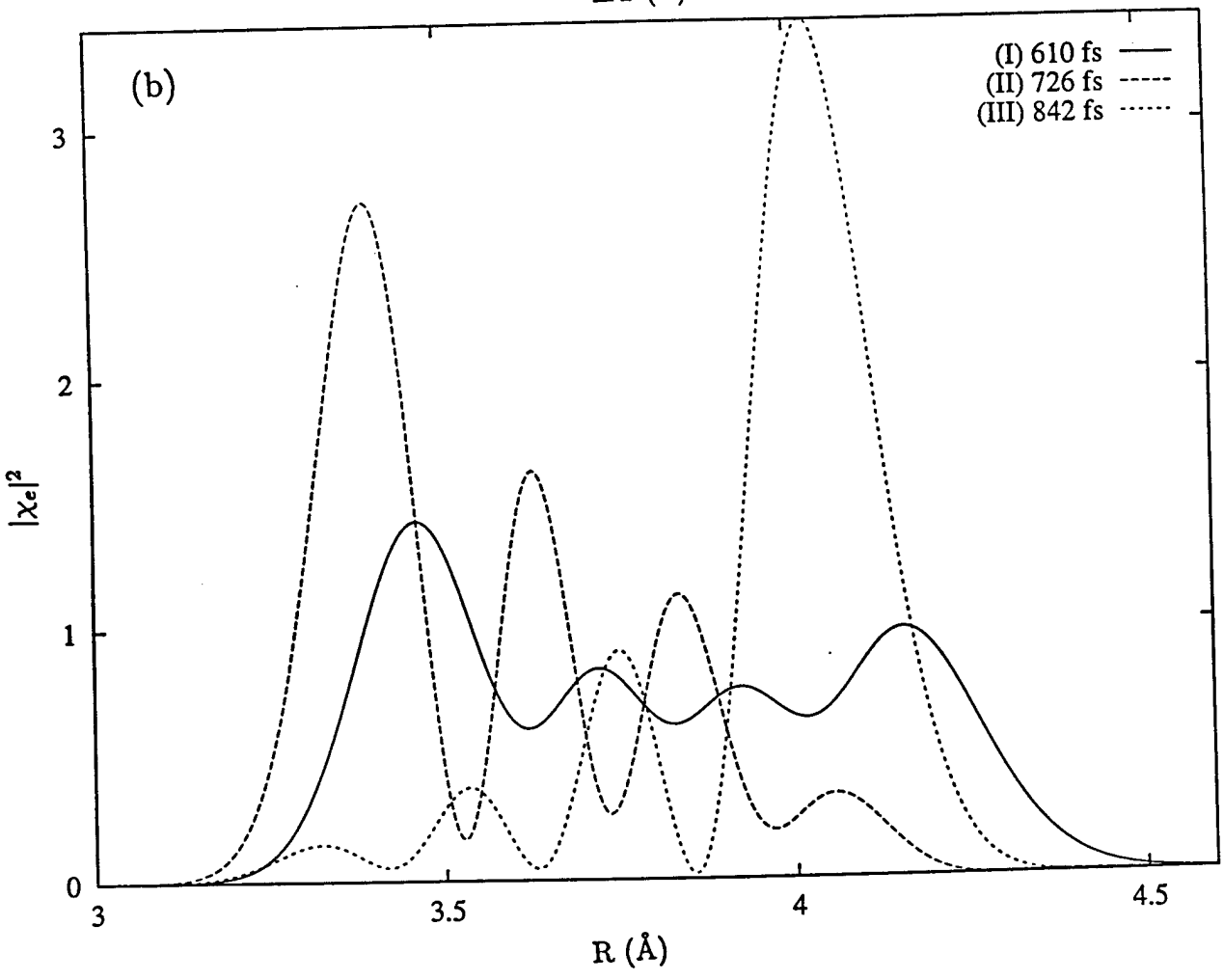
(b)
(I) 610 fs
(II) 726 fs
(III) 842 fs
$|\chi_e|^2$
3
2
1
0
3
3.5
4
4.5
R (Å)

Fig. 9

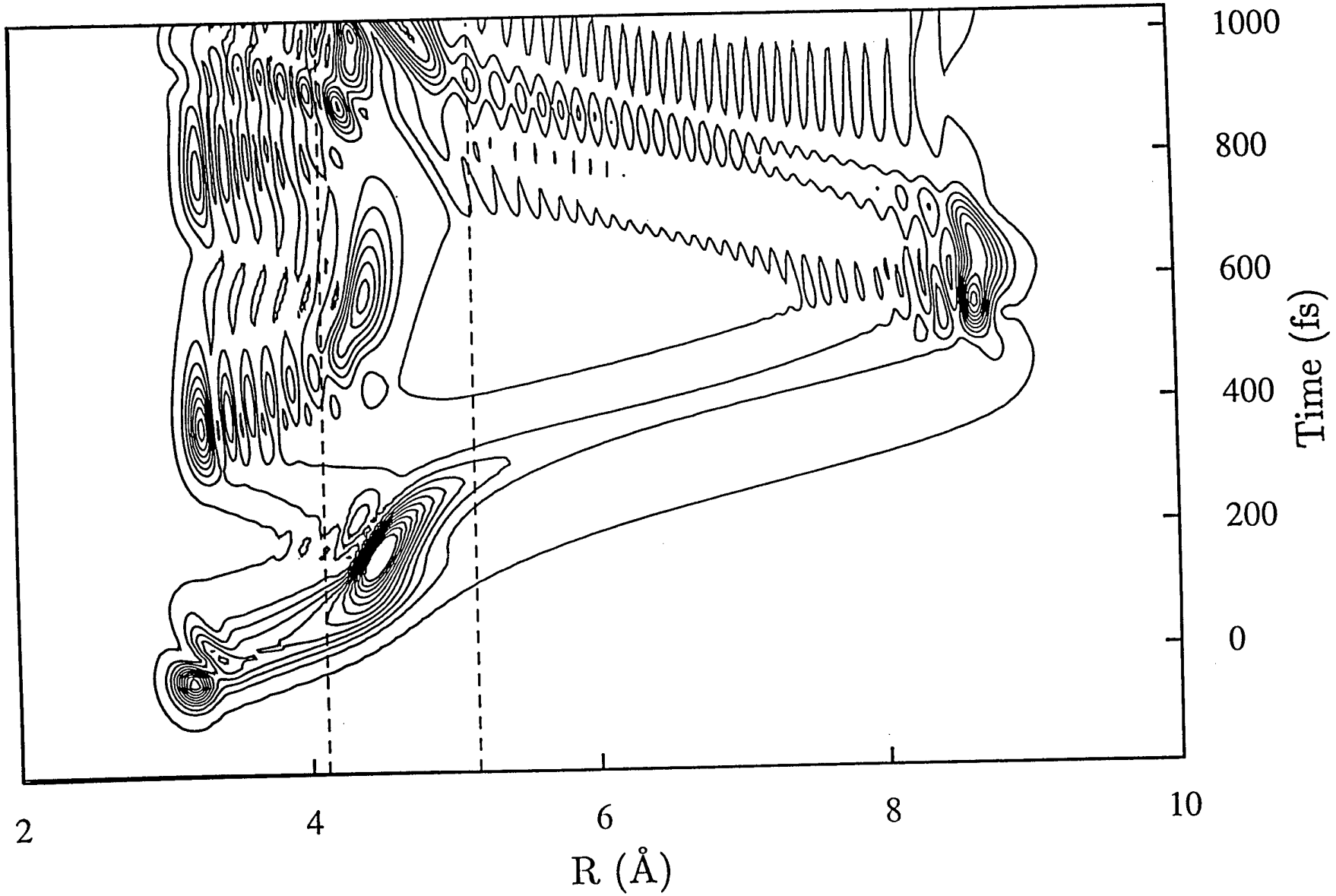

Fig. 10

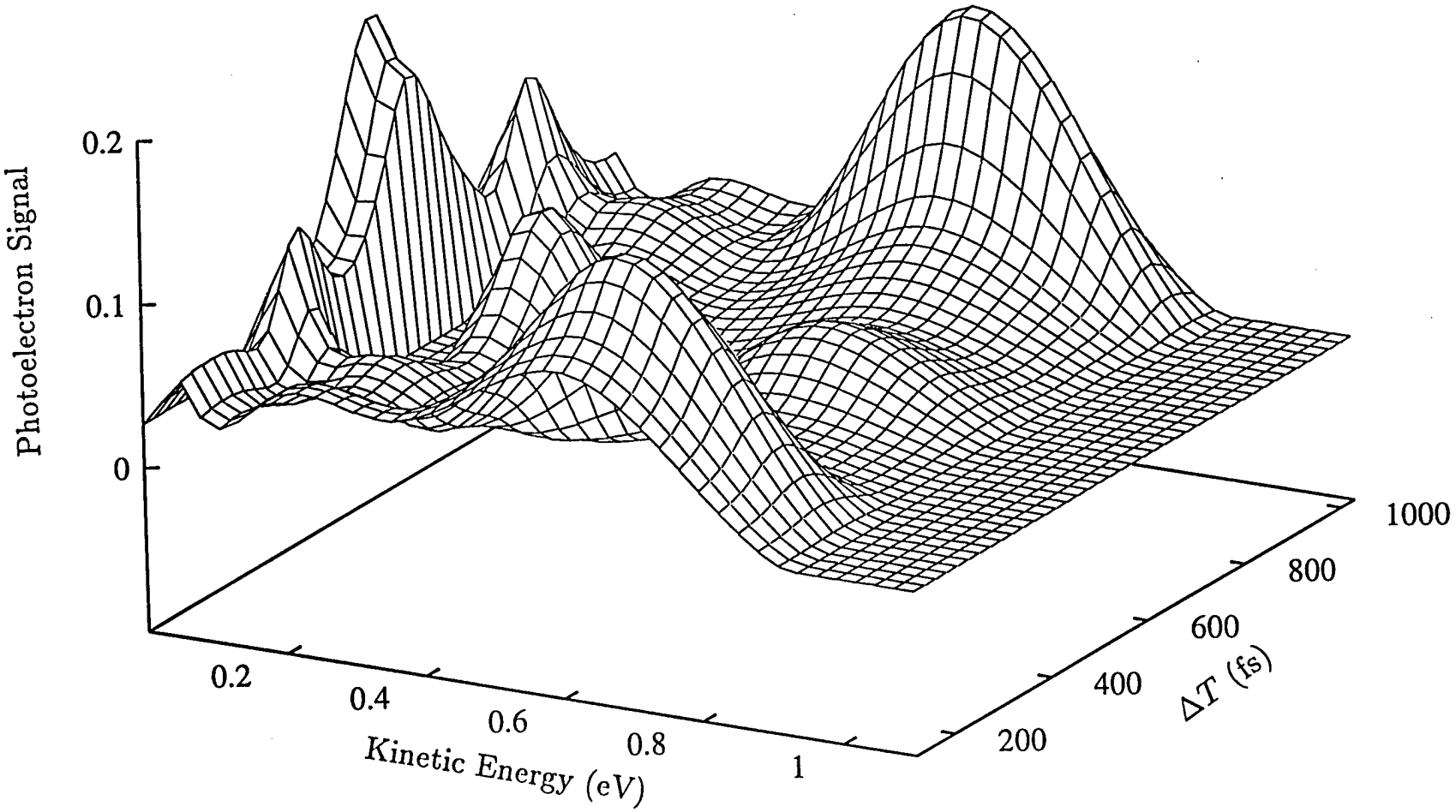
Photoelectron Signal
0.2
0.1
0
0.2
0.4
0.6
0.8
1
Kinetic Energy (eV)
200
400
600
800
1000
ΔT (fs)

Fig. 11

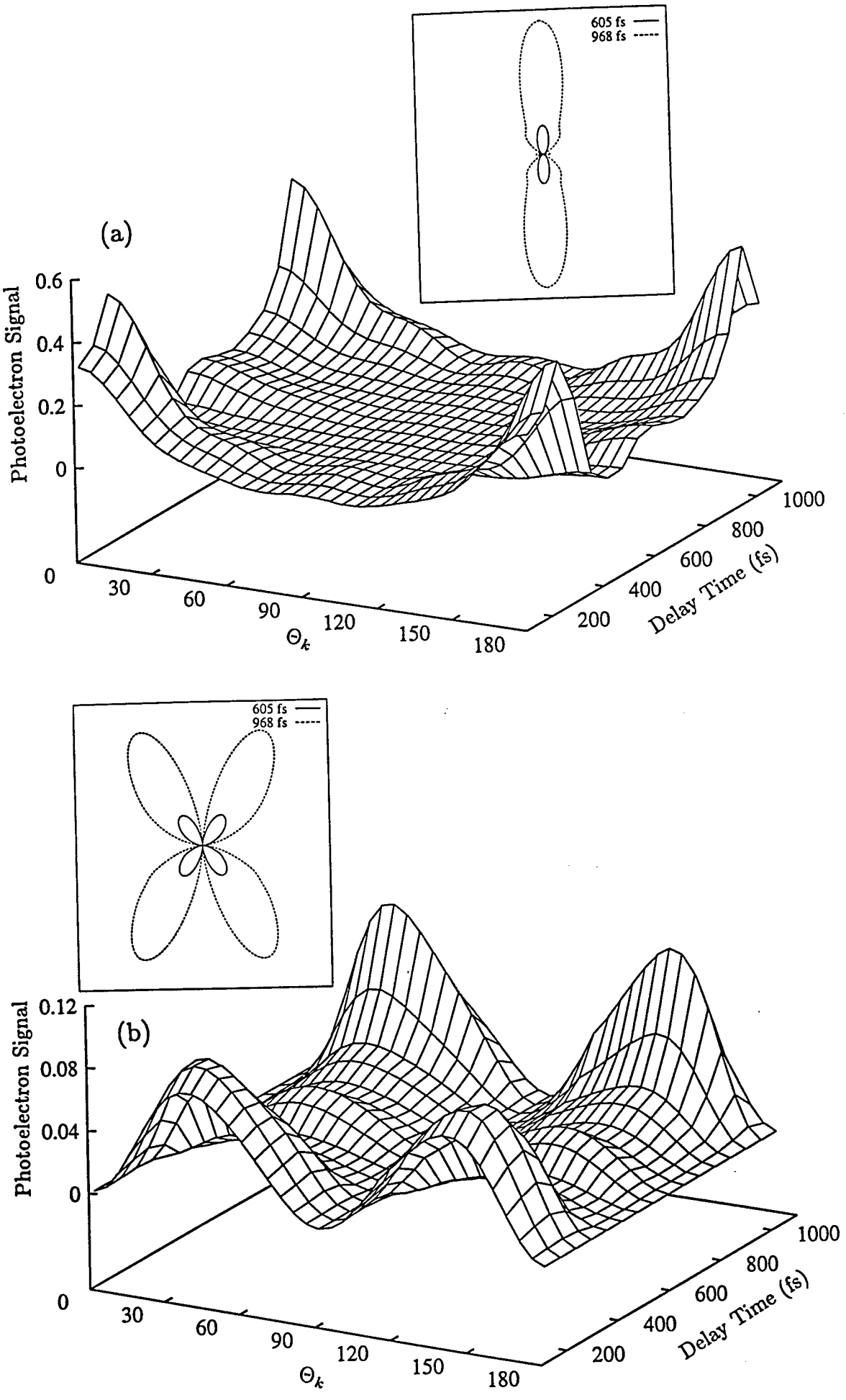
605 fs
968 fs
(a)
Photoelectron Signal
0.6
0.4
0.2
0
0
30
60
90
120
150
180
Θ_k
200
400
600
800
1000
Delay Time (fs)
605 fs
968 fs
(b)
Photoelectron Signal
0.12
0.08
0.04
0
0
30
60
90
120
150
180
Θ_k
200
400
600
800
1000
Delay Time (fs)

Fig. 12